Primordial gravitational wave probes of non-standard thermal histories

Marinichenko, Mariia

Primordial gravitational wave probes of non-standard thermal histories

THESIS

submitted in partial fulfillment of the
requirements for the degree of

MASTER OF SCIENCE
in
PHYSICS

Author :	Mariia Marinichenko
Student ID :	3747107
Supervisor :	Subodh Patil
Second corrector :	Ana Achúcarro

Leiden, The Netherlands, June 26, 2024

Primordial gravitational wave probes of non-standard thermal histories

Mariia Marinichenko

Instituut-Lorentz, Leiden University
P.O. Box 9500, 2300 RA Leiden, The Netherlands

June 26, 2024

Abstract

Primordial gravitational waves offer unique insights into the inflationary period and subsequent thermal history of the Universe. The spectrum of primordial high-frequency gravitational waves is highly sensitive to the processes in the early Universe and can be significantly suppressed during an epoch of early matter domination (EMD) induced by new long-lived massive particles. This damping effect is studied with numerical and analytic methods. The relative energy density of gravitational waves today is found to scale with the wavenumber k as $\Omega_{\rm GW} \propto k^{-2}$ for waves crossing the horizon during the EMD epoch. The overall damping between the start and the end of the EMD epoch is given by $m^{4/3}\Gamma^{-2/3}M_{Pl}^{-2/3}$, where m and Γ are the mass and decay width of the long-lived particles correspondingly, and M_{Pl} is the Planck mass. For concrete examples of EMD, models with inflaton decay and heavy neutral leptons are considered. Experimental observation of stochastic gravitational wave background could probe early cosmological events and constrain new physics scenarios.

Contents

Version of June 26, 2024 – Created June 27, 2024 - 16:33

Chapter 1

Introduction

The conventional cosmological paradigm is encapsulated in the ΛCDM model, which suggests that the Universe is isotropic, homogeneous, spatially flat, and filled with dark energy (cosmological constant Λ), cold dark matter (CDM), and baryonic matter. The model is based on three pillars: the expansion of the Universe, Big Bang nucleosynthesis (BBN), and the cosmic microwave background (CMB) [1]. BBN predicts the primordial abundances of light elements (H, D, He-3, He-4, Li-7), while the CMB provides a snapshot of the Universe when protons and electrons recombine into hydrogen atoms. Both phenomena occurred at temperatures of $\mathcal{O}(1)$ MeV and depend on the baryon-to-photon number density ratio $\eta_B \sim 6 \cdot 10^{-10}$. Observational probes are consistent with ΛCDM predictions [2, 3].

Despite the success of the ΛCDM model, the earliest evolution of the Universe remains one of the major mysteries of modern physics. Some hints about this period arise from cosmological problems in the hot Big Bang model: the horizon, flatness, and magnetic monopole problems. The horizon problem regards the uniformity of CMB temperature fluctuations in regions that were not in causal contact. The flatness problem concerns the almost zero curvature of the Universe, whose energy density increases over time. The magnetic monopole problem, relevant in Grand Unified Theory (GUT) scenarios, is based on the absence of magnetic monopoles, which should make a significant energy contribution. Those problems are naturally resolved with *inflation*, a brief period of accelerated expansion before radiation domination [4–6].

Inflation not only solves these Big Bang puzzles but also predicts a scale-invariant power spectrum of primordial density perturbations [7–9], confirmed by large-scale structure and CMB anisotropies [10]. An-

Version of June 26, 2024 – Created June 27, 2024 - 16:33

other prediction of inflation is the existence of *primordial gravitational waves* [11–13]. Their detection would prove the inflationary paradigm and provide insights into the early Universe. Due to their weak interaction with matter, primordial gravitational waves propagate through space-time almost undistorted, preserving precious information from epochs before BBN [14, 15]. However, changes in the effective number of relativistic degrees of freedom and neutrino free-streaming leave an imprint in the power spectrum of primordial gravitational waves, such as a 35.6% damping in amplitude due to neutrino anisotropic stress [16].

Detection of primordial gravitational waves is challenging due to their tiny amplitudes $h_{\mu\nu}$, which behaves like the second-order derivative of the quadrupole moment of energy density [17]. Indirect detection strategies focus on CMB B-mode polarization [18, 19], while direct detection relies on Michelson interferometry. In the latter method, a laser beam is split into two perpendicular arms, each with a test mass at the end. The beams travel along these arms and reflect off massive mirrors hanging from pendulums. A passing gravitational wave modifies arm lengths, causing monitorable changes in the interference pattern. LIGO and Virgo have detected gravitational waves with amplitudes of the order of 10^{-21} [20, 21]. To detect such tiny fluctuations, interferometers must have extremely large arms, typically several kilometers long. For ground-based observatories, the potential is limited by the Earth's size. However, in space-based detectors, the arms can reach millions of kilometers, measuring changes in distance between free-flying test masses via laser interferometry. For ground-based observatories, the potential is limited by the Earth's size. However, space-based detectors can have arms of millions of kilometers, significantly enhancing sensitivity.

Several powerful space interferometers were proposed for the detection of primordial gravitational waves, including the Deci-Hertz Interferometer Gravitational Wave Observatory (DECIGO) [22] and Big Bang Observer (BBO) [23], which are designed to observe frequencies around $f \sim 0.1 - 10$ Hz. Another important project is Laser Interferometer Space Antenna (LISA) [24] with a focus on lower frequencies of $10^{-5} - 1$ Hz. These bands correspond to crucial events in the early Universe, such as the reheating and phase transitions.

If primordial gravitational waves resulted from the one-field slow-roll inflation, their relative energy density is expected to be $\Omega_{GW} \sim 10^{-15} - 10^{-14}$ at $f \sim 1$ Hz [25]. With correlation analysis, optimized by co-aligned detectors, achievable sensitivity can be improved to $\Omega_{GW} \sim 10^{-16} - 10^{-15}$. The DECIGO/BBO project is to build two aligned detectors in the form of a star-of-David with two additional detectors. The resulting instrument

Version of June 26, 2024 – Created June 27, 2024 - 16:33

will have a long baseline ($L \sim 1$ AU) and high angular resolution.

Figure 1.1 shows the sensitivity curves for current and future gravitational wave detectors, including the constraints from the background noise. It highlights a promising frequency range around $f \sim 1$ Hz, which can be effectively probed by DECIGO and BBO. This frequency range offers valuable insights into the thermal history of the Universe immediately after inflation.

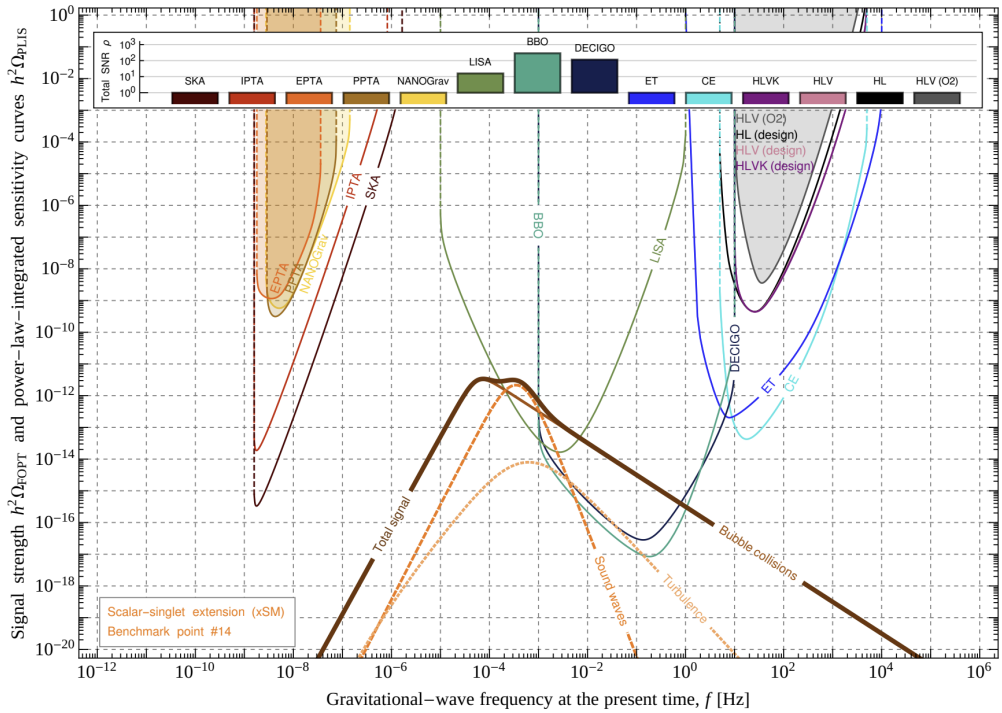

Figure 1.1: *Integrated sensitivity curves for current and future gravitational wave detectors. Signal-to-noise ratios are included in the panel on the top of the plot. Credit: [26].*

In this thesis, we examine the properties of *the stochastic primordial gravitational wave background* (SGWB) depending on various thermal histories, including "non-standard" cosmologies where the equation of state in the early Universe deviates from radiation. Specifically, we study scenarios with early matter domination (EMD), where the unstable massive particles decay into radiation. Our results indicate a prominent step-like feature in the power spectrum at small scales, regardless of the EMD timing and properties.

This thesis is organized as follows. In Chapter 2, we introduce the definitions and equations for describing primordial gravitational waves,

including the stochastic gravitational wave background, wave equation, and transfer function. Chapter 3 focuses on the radiation domination era, describing the effective number of relativistic degrees of freedom and neutrino decoupling. Chapter 4 concentrates on the power spectrum of primordial gravitational waves and its properties. Chapter 5 is dedicated to non-standard thermal histories, discussing inflation, reheating, and early matter domination. Chapter 6 presents the numerical solutions and analytical results. Finally, Chapter 7 summarizes our findings and provides conclusions. The appendices contain additional mathematical details, including Bessel functions, neutrino free-streaming, transfer functions, relative spectral density, and temperature evolution.

Version of June 26, 2024 – Created June 27, 2024 - 16:33

Chapter 2

Primordial gravitational waves

The essentials of General Relativity are captured by in the famous saying by John Archibald Wheeler: *"Spacetime tells matter how to move; matter tells spacetime how to curve."* In this framework, moving mass produces ripples in the fabric of spacetime, known as *gravitational waves* (GWs), which move with the speed of light c. These waves are solutions to *linearized* form of Einstein's equations.

GWs are produced by highly energetic cosmic events: mergers of compact binary systems (e.g., binary black holes and neutron stars), supernovae, rotating neutron stars (pulsars), and the events in the early Universe, that might produce an SGWB. This thesis focuses on the latter.

2.1 Stochastic gravitational wave background

Primordial gravitational waves are a fundamental prediction of any inflation model [11–13]. They are mainly produced by the growth of vacuum oscillations in the gravitational field during the rapid expansion of the Universe in the inflationary period. This process produces a nearly scale-invariant PGW spectrum with magnitude determined by the Hubble parameter during inflation. Another production option is the classical mechanisms, which involve interactions and perturbations, and contribute to SGWB production. These mechanisms introduce sources in the equation of motion for GWs, such as inflaton perturbations, scalar perturbations, and particle production. However second-order GWs produced by these classical mechanisms typically have smaller amplitudes than first-order quantum ones, they can still be significant in certain parameter ranges [27]. In this thesis, we consider the first-order primordial gravitational waves.

The importance of primordial gravitational waves lies in the valuable information they carry. Being weakly coupled to matter, they travel through spacetime with minimal distortion, preserving precious knowledge about the early Universe. PGW spectrum can probe epochs long before Big Bang Nucleosynthesis (BBN), offering insights into the inflation mechanism and physics at high energies and complementing energy-frontier collider searches for physics beyond the Standard Model (SM). In addition, the PGW spectrum facilitates an improved understanding of the thermal history of the Universe.

2.2 Wave equation

In linearized gravity applied to our Universe, the spacetime metric $g_{\mu\nu}(x)$ is expressed as the Friedmann-Lemaitre-Robertson-Walker (FLRW) metric with small perturbations $h_{\mu\nu}(x)$:

$$ds^2 = a^2(\tau)(-d\tau^2 + (\delta_{ij} + h_{ij})dx^i dx^j), \tag{2.1}$$

$$g_{\mu\nu}(x) = a^2(\tau)(\eta_{\mu\nu} + h_{\mu\nu}(x)), \quad |h_{\mu\nu}| \ll 1, \tag{2.2}$$

where $\eta_{\mu\nu}$ is the flat Minkowski metric.

Gravitational waves are solutions to Einstein's equations:

$$R_{\mu\nu} - \frac{1}{2}g_{\mu\nu}R = \frac{8\pi G}{c^4}T_{\mu\nu}, \tag{2.3}$$

where $R_{\mu\nu}$ is Ricci tensor, R is the Ricci scalar, G is the Newton's constant, and $T_{\mu\nu}$ is the stress-energy tensor.

In the linearized theory with curved spacetime, the propagation of gravitational waves becomes complex. It requires accounting for the background curvature $g_{\mu\nu}$ when computing derivatives. IBy expanding Eq. (2.3) to first order in $h_{\mu\nu}(x)$ in the *the Lorentz gauge*,

$$\partial^\mu \bar{h}_{\mu\nu} = 0, \tag{2.4}$$

we obtain

$$\Box_g \bar{h}_{\mu\nu} = -\frac{16\pi G}{c^4}T_{\mu\nu}, \tag{2.5}$$

where $\Box_g = \nabla^\mu \nabla_\mu$, and ∇_μ denotes the covariant derivative with respect to the background metric $g_{\mu\nu}$. The trace of $h_{\mu\nu}$ is denoted as $h = \eta^{\mu\nu}h_{\mu\nu}$, while $\bar{h}_{\mu\nu} = h_{\mu\nu} - \frac{1}{2}\eta_{\mu\nu}h$ is the trace-reversed perturbation. A detailed derivation of this equation is provided in [17].

Version of June 26, 2024 – Created June 27, 2024 - 16:33

This equation shows how gravitational waves interact with the curvature of spacetime, resulting in phenomena such as wave scattering and lensing by massive objects.

The Eq.(2.5) represents the system of ten equations for the perturbations $h_{\mu\nu}$. However, there are only two independent solutions. The Lorentz gauge imposes four constraints, but it does not uniquely define the gauge. The freedom in the choice of coordinates adds four more constraints. For studying gravitational waves effectively, we use the *the transverse-traceless* (TT) gauge. In this gauge, the perturbation $h_{\mu\nu}$ satisfies the conditions:

$$h_{0\mu} = 0, \quad \partial^i h_{ij} = 0, \quad h^i_i = 0. \tag{2.6}$$

These conditions demonstrate that $h_{\mu\nu}$ has only two independent components, corresponding to the two polarization states of gravitational waves.

To find the complete solution of Eq.(2.5), we need to specify both the metric and the initial conditions.

To examine the behavior of primordial gravitational waves throughout the history of the Universe, we calculate their amplitude in a Universe filled with matter and radiation. First, we derive the equation for amplitudes following the derivation from Watanabe et al. (2006) [28]. All the computations are done in natural units $c = \hbar = k_B = 1$.

For convenience, we use the transverse-traceless (TT) gauge without loss of generality. In this framework, gravitational waves have only two independent polarizations, conventionally denoted as $\lambda = +, \times$. These polarizations correspond to orthonormal tensors ϵ^λ_{ij}, satisfying $\epsilon^\lambda_{ij}\epsilon^\sigma_{ij} = 2\delta^{\lambda\sigma}$.. The amplitude is the linear combination:

$$h_{ij}(\tau, \mathbf{x}) = \sum_{\lambda=+,\times} \int \frac{d^3k}{(2\pi)^3} h_\lambda(\tau, \mathbf{k}) e^{i\mathbf{k}\cdot\mathbf{x}} \epsilon^\lambda_{ij}, \tag{2.7}$$

where $h_\lambda(\tau, \mathbf{k})$ is the Fourier component of perturbation with polarization λ.

Another important ingredient for calculations, the stress-energy tensor, is expressed as:

$$T_{ij} = p g_{ij} + a^2 \pi_{ij}, \tag{2.8}$$

where p is the pressure, and $\pi_{ij}(\tau, \mathbf{x})$ is anisotropic stress.

Isotropic stress $p g_{ij}$ does not enter the equation of motion for tensor perturbations and changes only the diagonal components of the metric, affecting the expansion rate of the Universe. However, the traceless and transverse anisotropic stress can be a source of gravitational waves. With

Version of June 26, 2024 – Created June 27, 2024 - 16:33

those considerations, we can write Eq. (2.5) as:

$$-\frac{1}{2}h^{;\nu}_{ij;\nu} = 8\pi G\pi_{ij}, \tag{2.9}$$

where zero-order terms were subtracted.

The explicit equation for each independent mode $h_\lambda(\tau, \mathbf{k}) \equiv h_{\lambda,\mathbf{k}}$ is

$$h''_{\lambda,\mathbf{k}} + \left(\frac{2a'}{a}\right) h'_{\lambda,\mathbf{k}} + k^2 h_{\lambda,\mathbf{k}} = 16\pi G a^2 \pi_{\lambda,\mathbf{k}}. \tag{2.10}$$

where $\pi_{\lambda,\mathbf{k}}$ is the Fourier component of anisotropic stress tensor.

2.3 Transfer function

In this section, we explore solutions to Eq. (2.10). For superhorizon fluctuations (where $k \ll Ha$), the right-hand side is negligibly smaller than the left-hand side, meaning that large waves do not feel processes on scales smaller than the Hubble radius. This simplifies the equation to:

$$\frac{h''_{\lambda,\mathbf{k}}}{h'_{\lambda,\mathbf{k}}} \approx -2\frac{a'}{a}. \tag{2.11}$$

The solution is

$$h_{\lambda,\mathbf{k}}(\tau) = A_1 + A_2 \int^\tau \frac{d\tau'}{a^2(\tau')}, \tag{2.12}$$

where A_1 and A_2 can be found from the initial conditions. The first term is of interest, while the last decreases as $a(\tau)$. With the expansion of the Universe, aH becomes smaller, and more modes re-enter the horizon. The solution can be extended to a general case, including evolution inside the horizon:

$$h_{\lambda,\mathbf{k}}(\tau) \equiv h^{\rm prim}_{\lambda,\mathbf{k}} \mathcal{T}(\tau, k), \tag{2.13}$$

where $h^{\rm prim}_{\lambda,\mathbf{k}}$ is the primordial gravitational wave mode when left the horizon during inflation. Here, we introduced the transfer function, $\mathcal{T}(\tau, k)$, satisfying $T(\tau, k) \to 1$ as $\tau \to 0$.

In the presence of neutrino free-streaming (see Section 3.2), the equation for the transfer function has the following form:

$$\mathcal{T}''(u) + 2\frac{a'(u)}{a}\mathcal{T}'(u) + \mathcal{T}(u) = -24 f_\nu(u) \left(\frac{a'(u)}{a}\right)^2 \int_{u_{\rm dec}}^u \frac{j_2(u-s)}{(u-s)^2}\mathcal{T}'(s)ds, \tag{2.14}$$

Version of June 26, 2024 – Created June 27, 2024 - 16:33

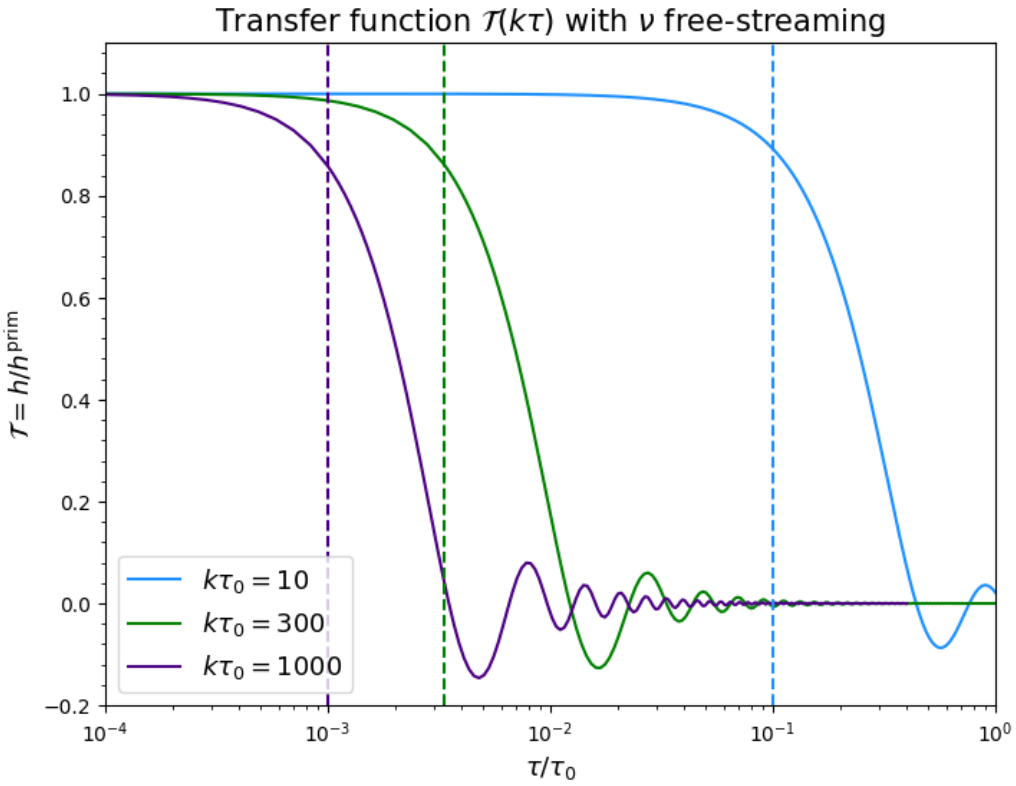

Figure 2.1: *Examples of transfer functions $\mathcal{T}(\tau, k)$ for modes crossing the horizon during RD and MD (indigo, green, and blue lines correspond to short, medium, and long wavelength modes), including neutrino free-streaming. Vertical dashed lines indicate entering the horizon. Short wavelengths experience more damping by the expansion of the Universe.*

where $u = k\tau$, $f_\nu(u)$ is the neutrino fraction in the total energy density, and $j_2(u)$ is the Bessel function (see Appendix A). Here and onwards $'$ denotes the derivative with respect to u. The derivation of this equation is provided in Appendix B, while analytical solutions with no anisotropic stress are presented in Appendix C.

The solutions of Eq. (2.14) are Bessel functions. Figure 2.1 shows transfer functions for modes crossing the horizon during matter domination (MD) and radiation domination (RD), while Figure 2.2 compares the numerical solution of $\mathcal{T}(k\tau)$ accounting for neutrino free-streaming with the analytical solutions from Appendix C. Figure 2.3 demonstrates the damping effect on the derivatives of the transfer function $\mathcal{T}'(k\tau)$ for modes entering the horizon shortly before neutrino decoupling.

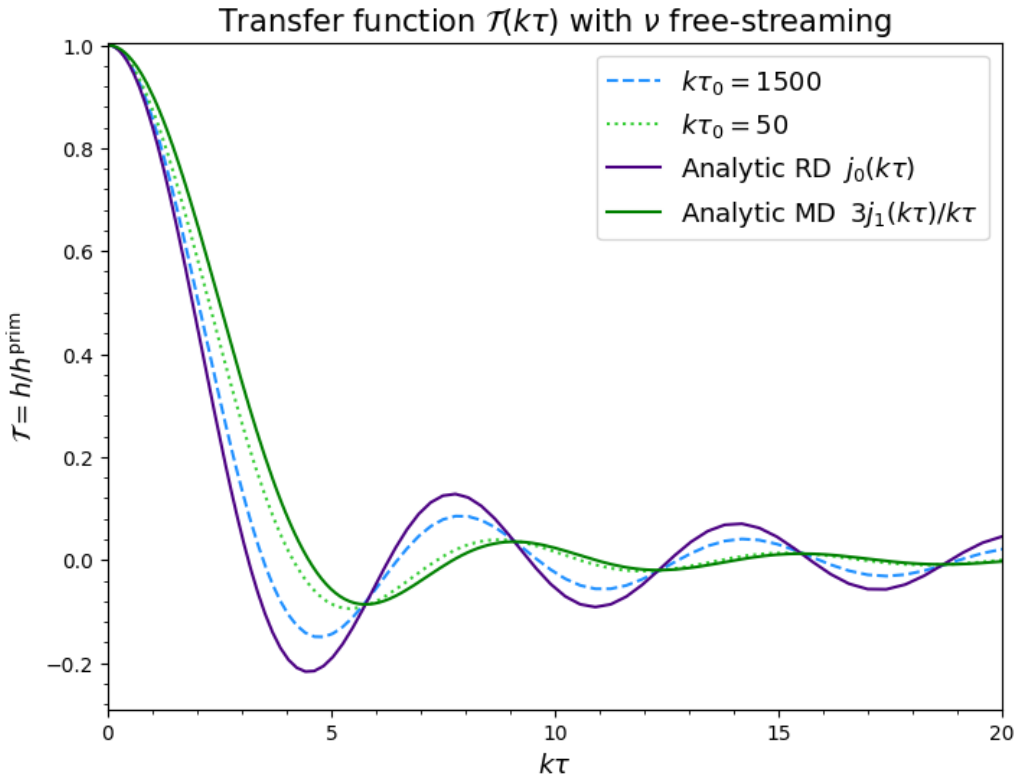

Figure 2.2: *Examples of transfer functions $\mathcal{T}(\tau, k)$ for modes crossing the horizon during RD ($k\tau_0 = 1500$) and MD ($k\tau_0 = 50$), where τ_0 is the present conformal time. Analytical solutions (solid lines) for RD and MD are provided for comparison. Numerical solutions (dashed and dotted lines) include neutrino free-streaming, causing noticeable damping for short-wavelength mode, which entered the horizon after neutrino decoupling.*

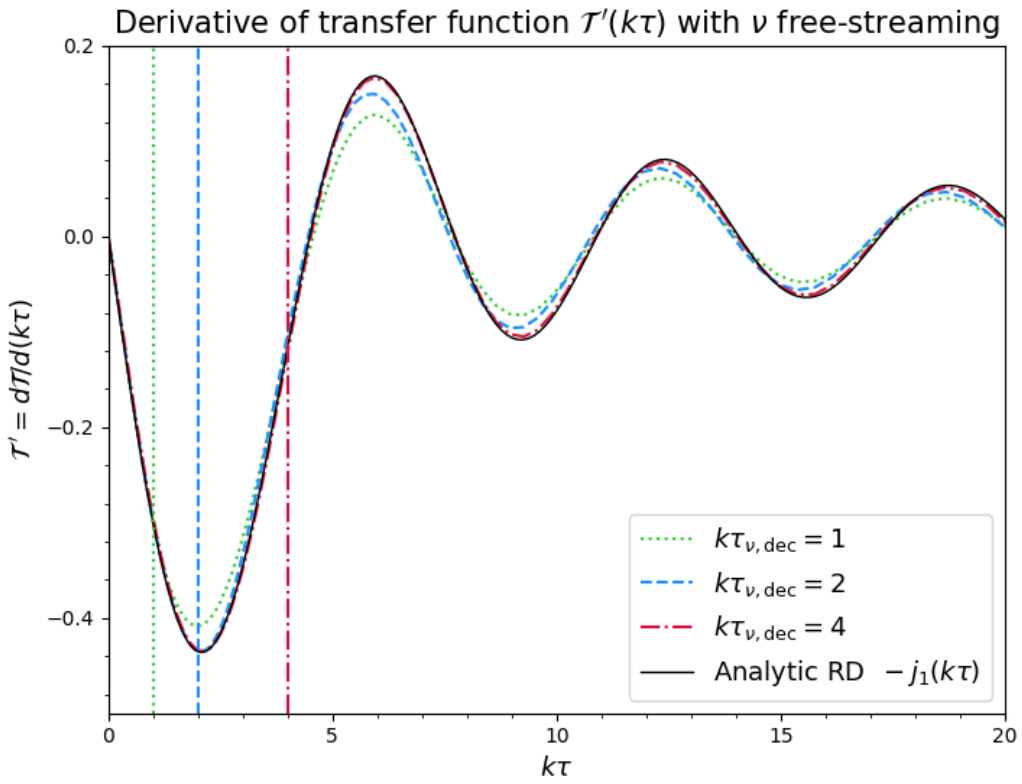

Figure 2.3: *Examples of derivatives of transfer functions $\mathcal{T}'(k\tau)$ for modes crossing the horizon shortly before the neutrino decoupling. Dotted, dashed, and dash-dotted lines correspond to $k = 1/\tau_{\nu,dec}$, $k = 2/\tau_{\nu,dec}$, and $k = 4/\tau_{\nu,dec}$, where $\tau_{\nu,dec}$ is the conformal time of neutrino decoupling. Analytical solution without neutrino free-streaming is represented by the solid black line. Vertical lines correspond to the moments of neutrino decoupling for each wavelength.*

Version of June 26, 2024 – Created June 27, 2024 - 16:33

Chapter 3

Radiation domination

Shortly after inflation, the Universe contains a hot plasma of elementary particles shown in Figure 3.1. During this RD, the energy density follows the law $\rho \propto a^{-4}$. However, this equation works only for a constant effective number of relativistic degrees of freedom. As the Universe cools down, some particles become non-relativistic. These changes affect the effective number of relativistic degrees of freedom, denoted as $g_\star$, which influences the radiation energy density ρ_R.

3.1 Effective number of relativistic degrees of freedom

To calculate the proper expression for $\rho_R(a)$, we start with entropy conservation, which connects equilibrium temperature T and scale factor a [29]:

$$s(T)a^3(T) = const, \qquad s(T) = \frac{2\pi^2}{45} g_{\star,s}(T) T^3, \tag{3.1}$$

$$T \propto a^{-1} g_{\star,s}^{-1/3}, \tag{3.2}$$

where $s(T)$ is the entropy per unit comoving volume:

$$s(T) = \frac{p+\rho}{T}, \qquad p(T) = \omega\rho(T), \tag{3.3}$$

and $g_{\star,s}$ is *the effective number of relativistic degrees of freedom* contributing to entropy. Here, $p(T)$ denotes pressure, and ω is the equation of state.

To calculate $g_\star$ and $g_{\star,s}$, we make simplifying assumptions. First, we assume that particles are in thermal equilibrium, implying that the interaction rate significantly exceeds the Hubble parameter. Second, we treat

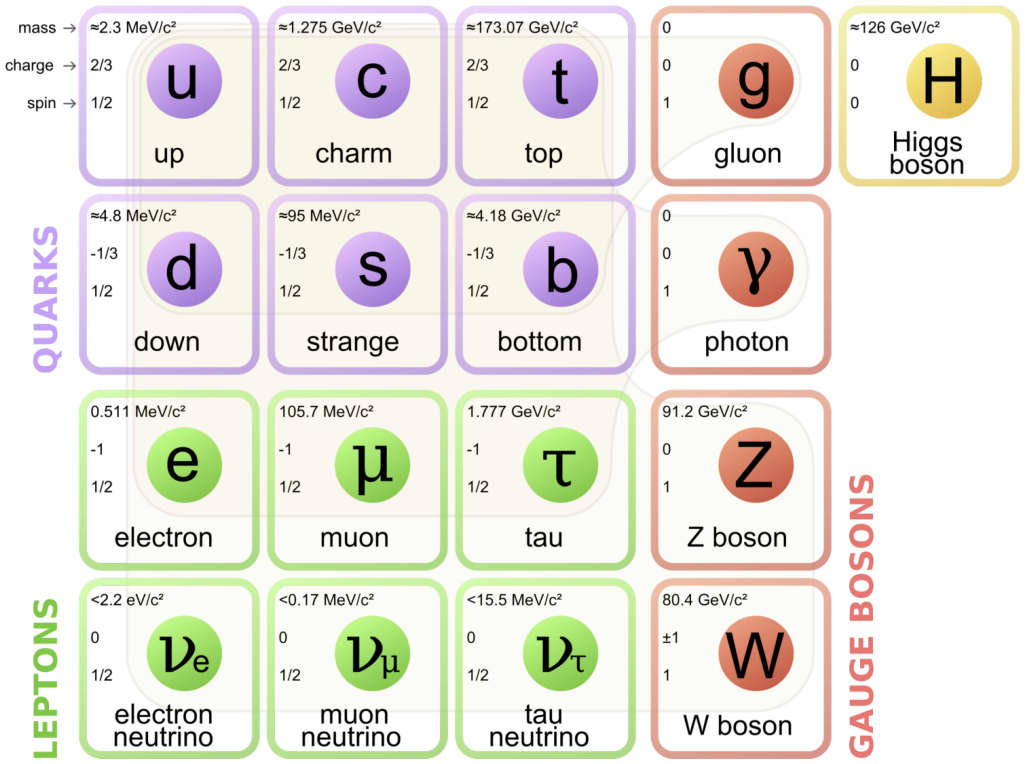

Figure 3.1: *Standard Model particles with their characteristics. Credit: Wikipedia.*

the system as an ideal gas, meaning that particle interactions through fundamental forces are negligible.

For species with mass m_i, the numbers of relativistic degrees of freedom are given by [29]:

$$g_{*,i}(T) = g_i \frac{15}{\pi^4} \int_{x_i}^{\infty} \frac{(u^2 - x_i^2)^{1/2}}{e^u \pm 1} u^2 du, \tag{3.4}$$

$$g_{*s,i}(T) = g_i \frac{15}{\pi^4} \int_{x_i}^{\infty} \frac{(u^2 - x_i^2)^{1/2}}{e^u \pm 1} \left(u^2 - \frac{x_i^2}{4} \right) du, \tag{3.5}$$

where $x_i = m_i/T$, g_i is the number of possible spin projections, and $"+"$ and $"-"$ refer to bosons and fermions correspondingly. Here, we assumed that there is no particle-antiparticle asymmetry, i.e. chemical potential μ_i is zero. The integration goes over $u = E/T$, where $E = \sqrt{\mathbf{p}^2 + m^2}$ is particle energy. Values of g_i for SM particles are listed in Table 3.1.

Table 3.1: *The Standard Model particles and their numbers of helicity states. Credit: L. Husdal, 2016 [30].*

Particle	Flavor	Antiparticle	Color	Spin	g_i
Quarks (u, d,c, s, t, b)	6	2	3	2	72
Charged leptons (e, μ, τ)	3	2	1	2	12
Pions ($\pi^{\pm}$, π^0)	1	2,1	1	1	3
Neutrinos (ν_e, ν_μ, ν_τ)	3	2	1	1	6
Gluons (g)	1	1	8	2	16
Photon (γ)	1	1	1	2	2
Massive bosons ($W^{\pm}$, Z^0)	2	2, 1	1	3	9
Higgs bosons (h)	1	1	1	1	1
All elementary particles	17				118

The total values of $g_\star$ and $g_{\star,s}$ are

$$g_*(T) = \sum_i g_{*,i}(T) \left(\frac{T_i}{T}\right)^4, \quad g_{*s}(T) = \sum_i g_{*s,i}(T) \left(\frac{T_i}{T}\right)^3, \tag{3.6}$$

where the sum goes over all the relativistic species i, each of which has its own temperature T_i that may differ from that of photons T.

These results are valid only when there are no interactions between different particle species. If such interactions occur, we need to consider these processes and perform particle simulations to compute $g_\star$ and $g_{\star,s}$. For simplicity, we will neglect these tiny corrections. However, examples of such calculations are given in [31, 32].

Once we have the correct temperature dependence $T(a)$, we can use it in the expression for entropy density $s(T)$:

$$\rho(T) = \frac{\pi^2}{30} g_\star(T) T^4, \qquad \rho(T) \propto g_\star g_{\star,s}^{-4/3} a^{-4}. \tag{3.7}$$

This result demonstrates how the change in the composition of relativistic plasma changes the radiation energy density. As a result, the scale factor a is also influenced by the solution of the Friedman equation:

$$a'(\tau) = H_0 \sqrt{\left(\frac{g_\star}{g_{\star,0}}\right)\left(\frac{g_{\star,s}}{g_{\star,s0}}\right)^{-\frac{4}{3}} \Omega_r + \Omega_m a}, \tag{3.8}$$

where Ω_m and Ω_r are normalized matter and radiation densities, and we have used $a_0 = 1$. Figure 3.2 shows the evolution of the Hubble parameter for constant and changing $g_\star$.

Version of June 26, 2024 – Created June 27, 2024 - 16:33

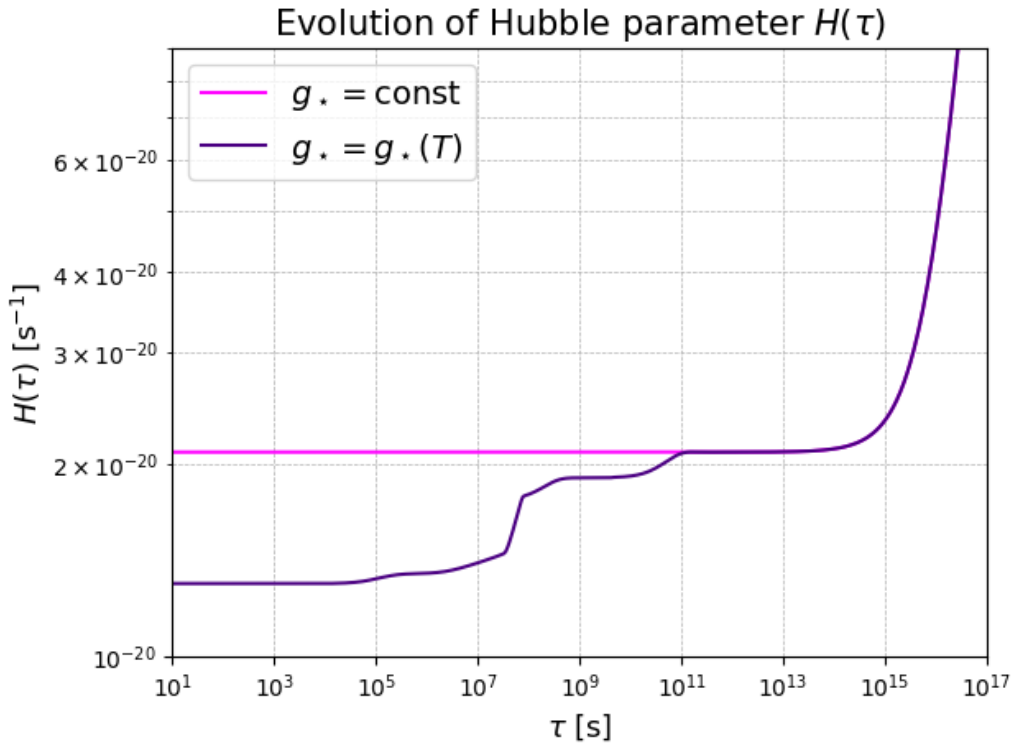

Figure 3.2: *Comparison of Hubble parameter evolution with constant $g_\star$ (magenta line) and varying $g_\star$ (indigo line).*

3.2 Neutrino decoupling

As the Universe cools and expands, particles must travel larger distances to interact. When the interaction rate, determined by the number density n and interaction cross section σ, becomes smaller than the expansion rate of the Universe H, interactions stop. This process is called *decoupling*.

For neutrinos, decoupling happened around $T \sim 1$ MeV, when the rate of weak interactions Γ_ν between neutrinos and electrons fell below the Hubble parameter:

$$\Gamma_\nu = n_e \langle \sigma v \rangle \approx T^3 (G_\mathrm{F} T)^2 \approx G_\mathrm{F}^2 T^5, \tag{3.9}$$

where n_e is the number density of electrons, σ and v are cross section and velocity for weak interactions, and $G_\mathrm{F} \approx 1.166 \cdot 10^{-5}\ \mathrm{GeV}^{-2}$ is the Fermi constant [30].

On the other hand, the Hubble parameter is

$$H = \sqrt{\frac{8\pi G}{3}\rho_R} \approx \sqrt{\frac{8\pi G}{3} g_\star(T) \frac{\pi^2}{30} T^4} \approx \sqrt{G T^4}, \tag{3.10}$$

where $G = M_{Pl}^{-2} = 6.9 \cdot 10^{-39}\ \mathrm{GeV}^{-2}$ is the Newton's constant.

The temperature of decoupling is

$$T_{\mathrm{dec}} \approx \left(\frac{\sqrt{G}}{G_F^2}\right)^{\frac{1}{3}} \approx 1\,\mathrm{MeV}. \tag{3.11}$$

After neutrino decoupling, another crucial event happened – electron-positron annihilation. Before decoupling, neutrinos and photons had the same temperature. However, new photons were created during annihilation, resulting in the increase in photon temperature $T_{\gamma,dec}$. The neutrino temperature T_ν can be computed as the function of the photon temperature T_γ:

$$T_\nu(T_\gamma) = \left(\frac{g_{\star,s}(T_\gamma)}{g_{\star,s}(T_{\mathrm{dec}})}\right)^{\frac{1}{3}} T_\gamma, \tag{3.12}$$

where we used the entropy conservation (3.1). Here, $g_{\star,s}(T_{\mathrm{dec}})$ is the effective number of relativistic degrees of freedom just before decoupling. This equation demonstrates that decoupling is not instantaneous, the numerator steadily varies with time. Using degeneracies from Table 3.1, we can compute T_ν when decoupling is finished:

$$T_\nu = \left(\frac{4}{11}\right)^{1/3} T_\gamma \approx 0.71 T_\gamma. \tag{3.13}$$

Figure 3.3 shows the evolution of effective degrees of freedom for entropy $g_{\star,s}$ and energy $g_\star$, accounting for all the processes mentioned before.

Version of June 26, 2024 – Created June 27, 2024 - 16:33

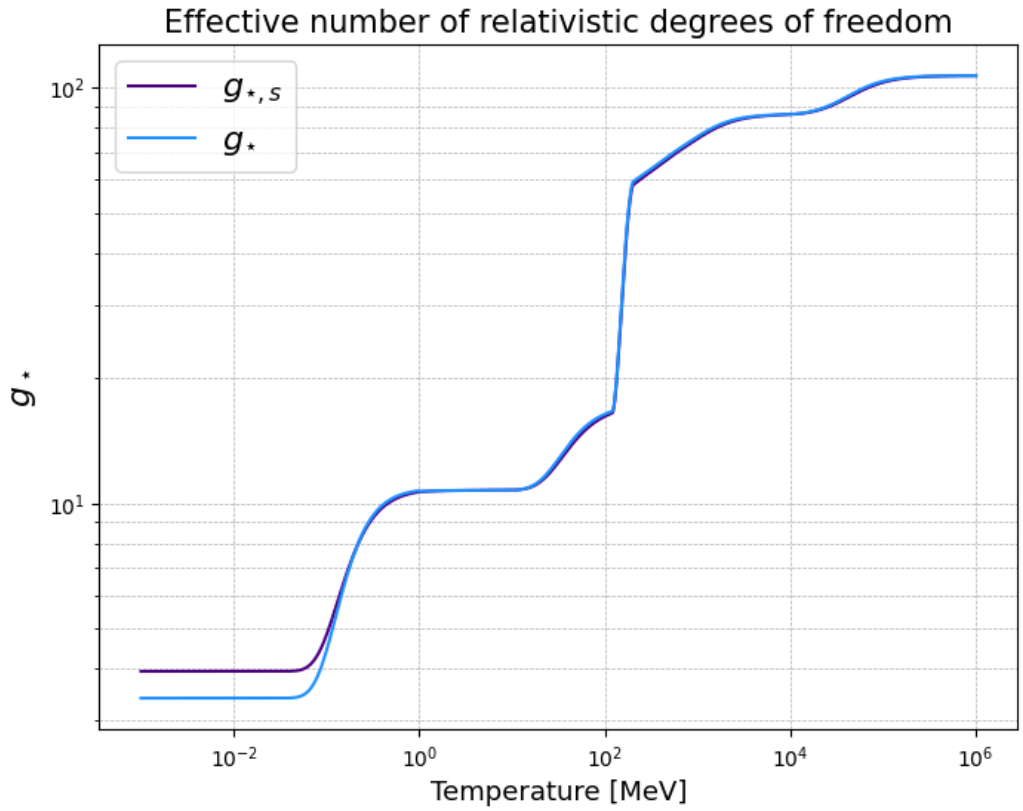

Figure 3.3: *Evolution of the effective number of relativistic degrees of freedom for energy density $g_\star(T)$ (blue) and entropy $g_{\star,s}(T)$ (indigo) as functions of equilibrium temperature T.*

Chapter 4

Energy density spectrum

The important characteristic of GWs is the energy they carry. This energy can be calculated using the effective stress-energy tensor $T_{\mu\nu}$, for the gravitational field. For a GW with perturbation $h_{\mu\nu}$, the energy density in the TT gauge is given by [17]:

$$\rho_{GW} = \frac{1}{32\pi G a^2(\tau)} \langle h'_{ij} h'^{ij} \rangle, \tag{4.1}$$

where the angle brackets represent averaging over multiple wavelengths. This expression shows that the energy density T_{00} is proportional to the square of the time derivative of the perturbation h'_{ij}, reflecting the wave-like nature of gravitational waves.

The power spectrum of primordial gravitational waves $\Delta^2_{GW}(\tau, k)$ is defined as:

$$\langle h_{ij}(\tau, \mathbf{x}) h^{ij}(\tau, \mathbf{x}) \rangle = \int \frac{dk}{k} \Delta^2_{GW}(\tau, k), \tag{4.2}$$

Performing an inverse Fourier transform gives:

$$\Delta^2_{GW}(\tau, \mathbf{k}) = \frac{2k^3}{2\pi^2} \sum_{\lambda} \langle |h_{\lambda,\mathbf{k}}(\tau)|^2 \rangle. \tag{4.3}$$

In this form, it becomes clear that the power spectrum depends only on the transfer function $\mathcal{T}(\tau, \mathbf{k})$, while other quantities relate to inflationary models:

$$\Delta^2_{GW,\text{prim}} = \frac{2k^3}{2\pi^2} \sum_{\lambda} \langle |h^{\text{prim}}_{\lambda,\mathbf{k}}|^2 \rangle = \frac{2}{\pi^2} \left(\frac{H_{\text{inf}}}{M_{\text{pl}}} \right)^2, \tag{4.4}$$

where H_{inf} is the Hubble parameter at the end of inflation ($\sim 10^{14}$ GeV), and $M_{\text{pl}} = 1.2 \cdot 10^{19}$ GeV is the Planck mass.

Generally, the value of $\Delta^2_{GW,\text{prim}}$ is analytically calculated for chosen inflationary models. However, it can alternatively be computed using the slow-roll approximation [33]:

$$r = \frac{\Delta^2_{GW,\text{prim}}}{\Delta^2_{S,\text{prim}}}, \tag{4.5}$$

where r is tensor-to-scalar ratio, and $\Delta^2_{S,\text{prim}}$ is the spectra of primordial scalar perturbations. Both parameters are constrained by combined CMB observations, galaxy clustering data, the latest supernovae measurements, and Lyman-alpha forest data.

The *relative spectral energy density* $\Omega_{GW}(\tau, k)$ is defined as:

$$\Omega_{GW}(\tau, k) \equiv \frac{\tilde{\rho}_{GW}(\tau, k)}{\rho_{\text{cr}}(\tau)} = \frac{\Delta^2_{GW,\text{prim}}}{12a^2(\tau)H^2(\tau)} |\mathcal{T}'(\tau, k)|^2, \tag{4.6}$$

where $\tilde{\rho}_{GW} = \frac{d\rho_{GW}}{d\ln k}$ is the energy density of gravitational waves. The complete derivation of this equation is given in Appendix D.

Since GWs are massless fields, their energy density depends on the scale factor similarly to radiation $\tilde{\rho}_{GW}(\tau, k) \propto a^{-4}$ for modes under the horizon $Ha \ll k$. Consequently, modes entering the horizon during the radiation epoch experience no suppression $\Omega_{GW}(\tau, k) = const$, and start to decay with the matter domination as $\Omega_{GW}(\tau, k) \propto a^{-1}$. Hence, modes entering the horizon at matter domination have smaller suppression.

The expressions for the relative spectral energy density, derived in Appendix C, are

$$\Omega_{GW}(\tau < \tau_{\text{eq}}, k > k_{\text{eq}}) = \frac{a^2 \Delta^2_{GW,\text{prim}}}{12 H^2_{\text{eq}} a^4_{\text{eq}}} k^2 [j_1(k\tau)]^2, \tag{4.7}$$

$$\Omega_{GW}(\tau > \tau_{\text{eq}}, k > k_{\text{eq}}) = \frac{a \Delta^2_{GW,\text{prim}}}{12 H^2_0 a^3_0} k^2 \frac{\tau^2_{\text{eq}}}{\tau^2} [A(k) j_2(k\tau) + B(k) y_2(k\tau)]^2, \tag{4.8}$$

$$\Omega_{GW}(\tau > \tau_{\text{eq}}, k < k_{\text{eq}}) = \frac{a \Delta^2_{GW,\text{prim}}}{12 H^2_0 a^3_0} k^2 \left[\frac{3 j_2(k\tau)}{k\tau}\right]^2, \tag{4.9}$$

where a_{eq} and H_{eq} are scale factor and Hubble parameter at the matter-radiation equality $\tau_{\text{eq}} \sim 10^{15}$ s, while $k_{\text{eq}} \sim 10^{-15}$ Hz is the wavenumber of

Version of June 26, 2024 – Created June 27, 2024 - 16:33

the mode entering the horizon at that moment. H_0 and a_0 denote present time values. Functions $j_1(x)$, $y_1(x)$, and $j_2(x)$ are spherical Bessel function, whose expressions are given in Appendix A.

Eq.(4.7) corresponds to energy density at RD epoch, while Eq.(4.8) and Eq.(4.9) describe Ω_{GW} during the MD epoch for modes that entered horizon before and after matter-radiation equality, respectively. For large values of the combination $k\tau$, coefficients $A(k)$ and $B(k)$ in Eq.(4.8) behave as k^{-1}, explaining the flattening in the spectrum. Conversely, for modes that entered the horizon at matter domination $\Omega_{GW}(\tau, k) \propto k^{-2}$, resulting in a peak at small k.

To extract information about events preceding BBN, we need to examine the high-frequency part of the spectra. Up to this point, we assumed that $\rho \propto a^{-4}$ at RD epoch. However, this relation does not always hold. In the previous chapter, we mentioned that $\rho_{\rm cr} = \rho_r \propto g_\star g_{\star,s}^{-4/3} a^{-4}$ for RD, while the energy density of GWs stays $\rho_{GW} \propto a^{-4}$ inside the horizon ($Ha \ll k$). Consequently, for modes entering the horizon during the radiation domination, the relative contribution to energy density is

$$\Omega_{GW}(\tau_0, k > k_{\rm eq}) = \Omega_{GW}(\tau_{\rm hc}, k)\Omega_{r0} \left(\frac{g_{*s}(T_{\rm hc})}{g_{*s0}}\right)^{-4/3} \left(\frac{g_*(T_{\rm hc})}{g_{*0}}\right), \quad (4.10)$$

where T_{hc} and $\tau_{hc} < \tau_{\rm eq}$ are the equilibrium temperature and conformal time during horizon crossing.

Eq.(4.10), demonstrates that the sooner the mode enters the horizon, the more significant it is suppressed due to the monotonic decrease of $g_\star$ and $g_{\star,s}$. Interestingly, these two quantities have the same values up to temperatures around $T \sim 0.1$ MeV, where neutrinos decouple. Then the decrease ceases, and the behavior of $\Omega_{GW}(\tau_0, k > k_{\rm eq})$ is described by Eq.(4.8).

Figure 4.1 shows $\Omega_{GW}(\tau_0, k)$ across frequencies from soon post-inflation horizon entry to present, for both constant and varying $g_\star$. Figure 4.2 zooms in on frequencies corresponding to significant events during RD.

The relation between the temperature at the moment of horizon crossing $T_{\rm hc}$ and the present frequency of the gravitational wave f_0 can be derived using the definition of wavelength at horizon crossing $k_{\rm hc} = H_{\rm hc} a_{\rm hc}$, entropy conservation (3.1), and the Friedman equation expressed in terms of temperature (3.10). The result is [28, 34]:

$$f_0 = 1.65 \times 10^{-7} \left(\frac{T_{\rm hc}}{1\,\text{GeV}}\right) \left(\frac{g_{*\rm s}(T_{\rm hc})}{100}\right)^{-1/3} \left(\frac{g_*(T_{\rm hc})}{100}\right)^{1/2} \text{Hz}, \quad (4.11)$$

Version of June 26, 2024 – Created June 27, 2024 - 16:33

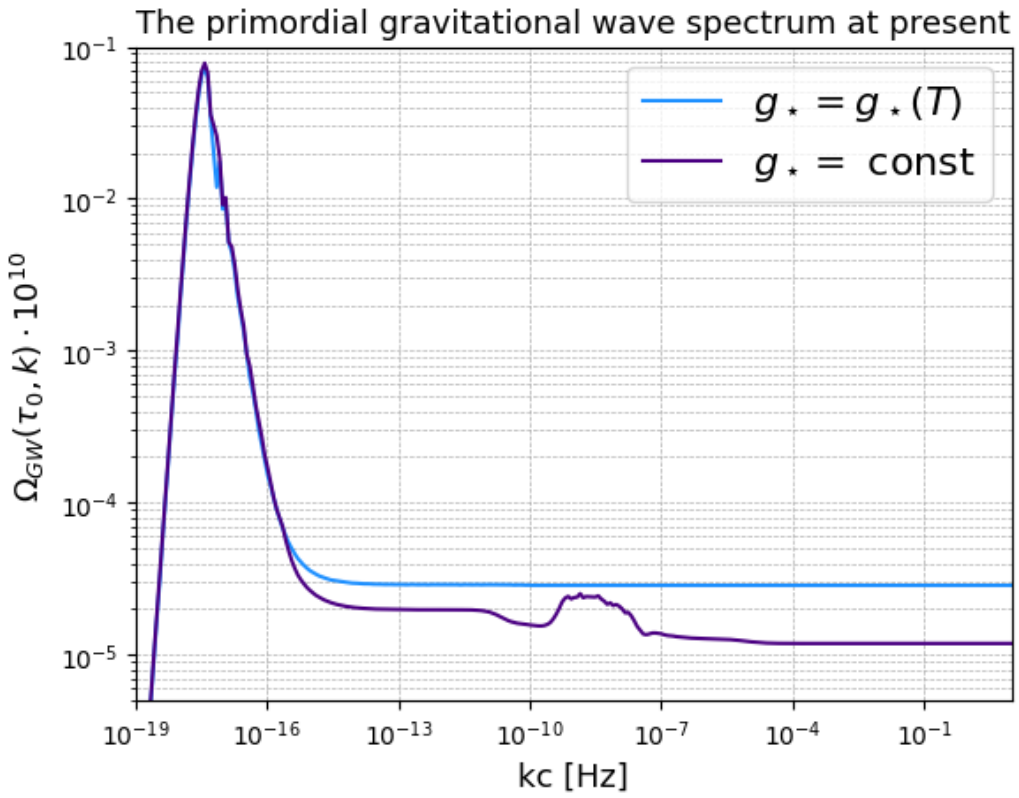

Figure 4.1: *Spectrum of primordial gravitational waves at $\tau = \tau_0$ as the function of comoving wavelength k (frequency kc in Hz). The blue line corresponds to a constant effective number of relativistic degrees of freedom $g_\star$, while the indigo line accounts for changes in $g_\star$ and neutrino decoupling.*

Version of June 26, 2024 – Created June 27, 2024 - 16:33

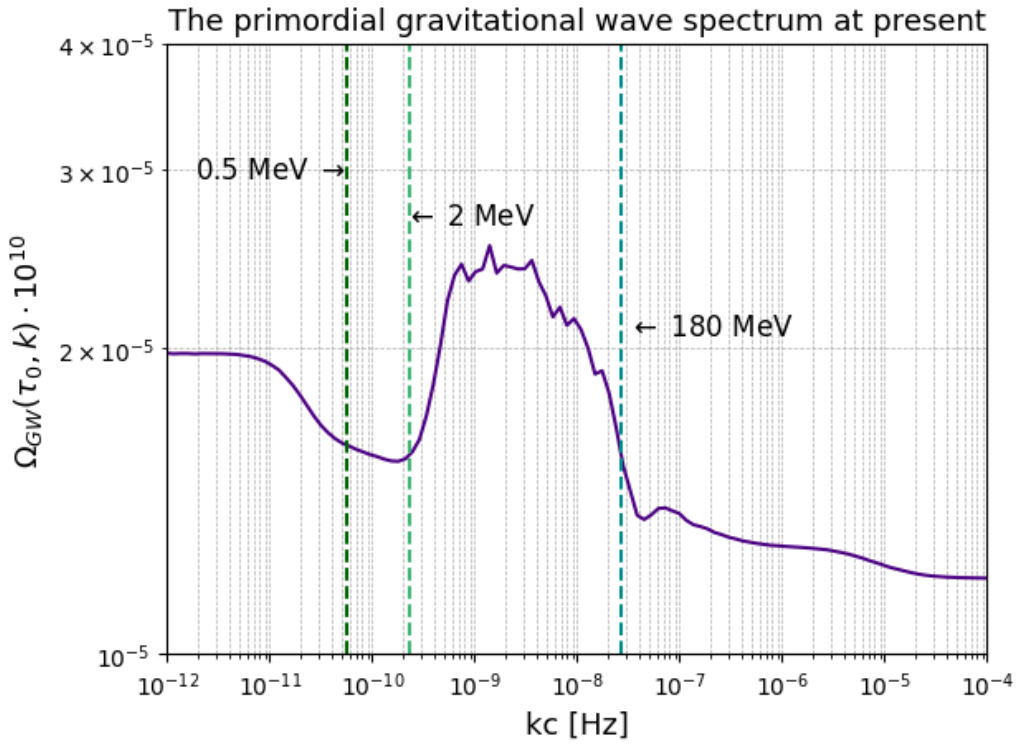

Figure 4.2: *Zoomed-in part of PGW spectrumfrom Figure 4.1, highlighting key transitions during radiation domination. Dashed vertical lines mark QGP phase transition (*180 *MeV), neutrino decoupling* 2 *MeV, and* e^+e^- *annihilation (*0.5 *MeV).*

Chapter 5

Non-standard thermal histories

According to the cosmological standard model, the Universe was radiation-dominated after inflation. While cooling, it switched to matter dominance. However, this is not the only scenario consistent with observations. Currently, there are no observational probes of the Universe prior to BBN, meaning that radiation domination at earlier times is not confirmed [35]. It leaves a possibility that the Universe experienced an additional phase of early matter domination before the conventional RD. For example, massive metastable particles dominating the energy density of the Universe immediately after inflation could lead to scenarios involving early radiation and matter domination epochs. Another alternative is a slow reheating phase. There are multiple scenarios for the evolution of the Universe between inflation and BBN, the elaborate review was done by Allahverdi et al. (2020) [36]. In this thesis, we will focus on the dynamics with additional massive decaying particles (e.g., inflaton).

Non-standard thermal histories have a significant impact on the amplitude and polarization of primordial gravitational waves [37]. Consequently, the constraints on the observed parameters of the primordial gravitational wave power spectrum are explicitly related to the parameters governing the evolution of the Universe prior to BBN.

5.1 Inflation and reheating

In the conventional inflationary scenario, most elementary particles were created during the *reheating* phase [38]. During inflation, the slowly changing inflaton field constitutes all the energy in the Universe. In this section, we consider the simplest case with the only minimally coupled inflaton

field φ, described by the Lagrangian:

$$\mathcal{L} = -\frac{1}{2}\partial_\mu\varphi\partial^\mu\varphi - V(\varphi), \tag{5.1}$$

where $V(\varphi)$ is the potential energy of inflaton field φ.

The stress-energy tensor of the inflaton field is

$$T_{\mu\nu} = -2\frac{\partial\mathcal{L}}{\partial g^{\mu\nu}} + g_{\mu\nu}\mathcal{L} = \partial_\mu\varphi\partial_\nu\varphi + g_{\mu\nu}\left(-\frac{1}{2}g^{\alpha\beta}\partial_\alpha\varphi\partial_\beta\varphi - V(\varphi)\right). \tag{5.2}$$

this expression tells us that φ behaves as a perfect fluid with the energy density and pressure:

$$\rho_\varphi = \frac{\dot{\varphi}^2}{2} + V(\varphi), \quad p_\varphi = \frac{\dot{\varphi}^2}{2} - V(\varphi), \tag{5.3}$$

where $\dot{}$ denotes the derivative with respect to the time t. The equation of state is then

$$\omega_\varphi = \frac{\dot{\varphi}^2 - 2V(\varphi)}{\dot{\varphi}^2 + 2V(\varphi)} = \frac{n-1}{n+1}, \tag{5.4}$$

where we chose the effective potential in the form $V(\varphi) \propto |\varphi|^{2n}$. In general, this parameter can take any value from $-1 \leq \omega_\varphi \leq 1$. For $n = 1$, the field behaves as matter, while for $n = 2$ it behaves as radiation. However, not all values lead to accelerated expansion. The acceleration of the Universe is defined by the second Friedmann equation:

$$\frac{\ddot{a}}{a} = -\frac{4\pi G}{3}(\rho + 3p). \tag{5.5}$$

To have accelerated expansion of the Universe, the inflaton field must satisfy the following equality:

$$\rho_\varphi + 3p_\varphi = 2\left(\dot{\varphi}^2 - V(\varphi)\right) < 0, \qquad V(\varphi) > \dot{\varphi}^2. \tag{5.6}$$

To get exponential expansion, the energy density of φ must be dominated by potential energy:

$$\dot{\varphi}^2 \ll V(\varphi). \tag{5.7}$$

The most straightforward realization of this condition is the inflaton field slowly moving to the minimum of $V(\varphi)$. Figure 5.1 contains the example of the slow-roll potential.

The Euler-Lagrange equation for $\varphi(t)$ is the Klein-Gordon equation, which in the FLRW has the following form

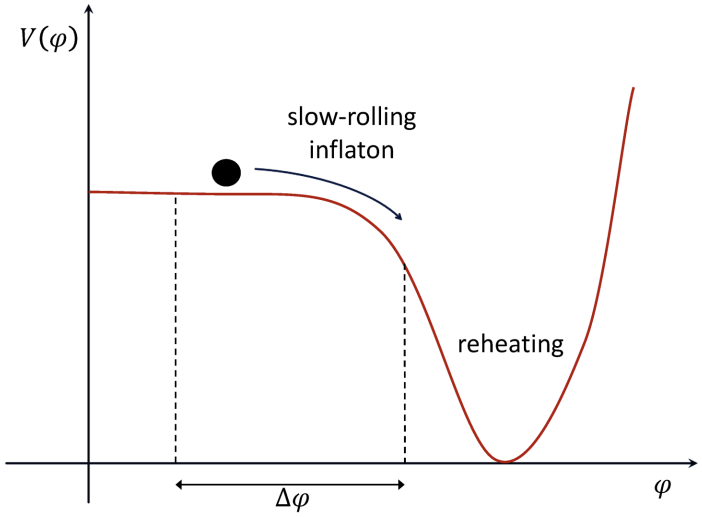

Figure 5.1: *Example of slow-roll inflation potential. Credit: Guzzetti et al., 2016 [27].*

$$\ddot{\varphi} + 3H\dot{\varphi} + V'_{\varphi}(\varphi) = 0, \tag{5.8}$$

where we took into account that the inflaton field is homogeneous during the inflation.

Initially, φ is large ($\varphi > M_{pl}$), and the dynamic of the inflaton field is governed by the "friction" term $3H\dot{\varphi}$. The Hubble parameter, given by

$$H^2 = \frac{8\pi G}{3}\left(\frac{\dot{\varphi}^2}{2} + V(\varphi)\right) \tag{5.9}$$

is dominated by the nearly constant inflaton potential energy $V(\varphi)$ during inflation, resulting in quasi-exponential expansion of the Universe.

The slow-roll conditions can be expressed in the compact form:

$$\epsilon \equiv \frac{M_{\rm pl}^2}{2}\left(\frac{V'_{\varphi}}{V}\right)^2 \ll 1, \tag{5.10}$$

$$\eta \equiv M_{\rm pl}^2 \frac{V''_{\varphi\varphi}}{V} \ll 1, \tag{5.11}$$

where ϵ and η are slow-roll parameters [39].

Inflation ends when the inflaton field rapidly rolls toward the minimum of the effective potential, leading to oscillations near it. This transition from the inflation phase to the hot Big Bang is known as *reheating*

[40]. During reheating, the inflaton field produces elementary particles, which interact and establish thermal equilibrium. As the oscillations of the inflaton field decrease in amplitude, the energy of φ is transferred to these new relativistic particles. Reheating ends when this energy transfer is complete, defining the equilibrium temperature at that moment $T_{\rm reh}$ – reheating temperature.

The equation of motion for φ with the quadratic potential $V(\varphi) = \frac{1}{2}m_\varphi^2\varphi^2$, during reheating is the Klein-Gordon equation:

$$\ddot{\varphi} + (3H(t) + \Gamma_\varphi)\dot{\varphi} + m_\varphi^2\varphi = 0, \tag{5.12}$$

where m_φ is the inflaton mass, and Γ_φ is its the decay rate. This equation can be used only for rapid oscillations of φ.

The solution of the equation (5.12) can be written as

$$\varphi(t) = \Phi(t)e^{-im_\varphi t}, \tag{5.13}$$

where $\Phi(t)$ is the amplitude of inflaton field, and e^{-imt} is the oscillatory part. Then energy density ρ_φ and number density n_φ of φ are

$$\rho_\varphi = \frac{1}{2}m_\varphi^2\Phi^2, \qquad n_\varphi = \frac{1}{2}m_\varphi\Phi^2. \tag{5.14}$$

The equation of motion (5.12) can be expressed in terms of amplitude $\Phi(t)$:

$$\frac{1}{a^3}\frac{d}{dt}(a^3\Phi^2) = -\Gamma_\varphi\Phi^2, \tag{5.15}$$

which has a straightforward interpretation in terms of energy density:

$$\frac{d}{dt}(a^3\rho_\varphi) = -\Gamma a^3\rho_\varphi. \tag{5.16}$$

This indicates that the total comoving energy density decays exponentially with Γ_φ.

The end of reheating occurs, when the rate Γ_φ becomes smaller than the expansion rate H:

$$H \sim \Gamma_\varphi \qquad \Longrightarrow \qquad \rho(t_{\rm reh}) \approx \frac{3\Gamma^2 M_{pl}^2}{8\pi}. \tag{5.17}$$

The energy density of early RD Universe is

$$\rho(t_{\rm reh}) \approx \frac{3\Gamma_\varphi^2 M_{pl}^2}{8\pi} \approx \frac{\pi^2 g_\star}{30}T_{\rm reh}^4, \tag{5.18}$$

which is valid under the assumption of the instantaneous equilibrium after the reheating. At this time, all particles from Table 3.1 are relativistic, which implies $g_\star \sim 10^2 - 10^3$. The simple estimate for the resulting reheating temperature is [40]

$$T_{\rm reh} \approx 0.2\sqrt{\Gamma_\varphi M_{pl}}, \tag{5.19}$$

which shows that $T_{\rm reh}$ depends only on the particle model of φ.

5.2 Early matter domination

When inflatons are heavy, they become non-relativistic before their decay. This results in early radiation and matter domination epochs before φ decays into SM particles.

The dynamics of two dominant components, radiation R and inflaton field φ, is described by the two coupled Boltzmann equations [35, 41]:

$$\frac{d\rho_\varphi}{dt} + 3H\rho_\varphi = -\Gamma_\varphi \rho_\varphi, \tag{5.20}$$

$$\frac{d\rho_R}{dt} + 4H\rho_R = \Gamma_\varphi \rho_\varphi, \tag{5.21}$$

where ρ_R is the energy density of relativistic particles defined in Eq.(3.7), and T is the temperature of the Universe. The Hubble parameter is defined by the Friedman equation:

$$H^2 = \frac{8\pi G}{3}\left(\rho_\phi + \rho_R + \rho_m + \rho_\Lambda\right), \tag{5.22}$$

where ρ_R was defined in Eq.(3.7), and ρ_m and ρ_Λ are energy densities of matter and the cosmological constant, which comprise a tiny fraction of the energy budget of the Universe.

To complete the system, we should add the equation of the evolution of the energy density of matter:

$$\frac{d\rho_m}{dt} + 3H\rho_m = 0, \tag{5.23}$$

which becomes relevant at later times.

The decay width Γ_φ can be expressed in terms of reheating temperature $T_{\rm reh}$ using Eq.(5.17):

$$\Gamma_\varphi = \sqrt{\frac{4\pi^3 g_\star(T_{\rm reh})}{45}}\frac{T_{\rm reh}^2}{M_{pl}}. \tag{5.24}$$

The value of T_{reh} is constrained by BBN, requiring precise parameters. One of those parameters is the contribution to the effective number of relativistic degrees of freedom from neutrinos $N_{eff} = 3.046$, which largely impacts the evolution of the scale factor a. Moreover, electron neutrinos alter the neutron-proton balance. As a result, the T_{reh} must be greater than BBN temperature to have time for neutrino thermalization: $T_{\text{reh}} \gtrsim T_{\text{BBN}}$ [42–45]. In our analysis, we will consider different values of T_{reh} and study their impact on the PGW spectrum.

Conservation of total comoving energy allows calculation of temperature evolution. The energy transfer $\Gamma_\varphi \rho_\varphi$ from φ to radiation adds a term to the differential equation relating temperature T and scale factor a:

$$\frac{dT}{da} = \left[1 + \frac{T}{3g_{\star,s}}\frac{dg_{\star,s}}{dT}\right]^{-1}\left[-\frac{T}{a} + \frac{\Gamma_\varphi \rho_\varphi}{3H(a)s_R(T)a}\right]. \tag{5.25}$$

The details of the derivation of this equation are in Appendix E.

Solving the system of Eq.(5.20) combined with Eq.(5.25) provides the temperature evolution $T(a)$ during reheating. The expansion rate is then calculated from Eq.(5.22).

In a simple case with no change in the number of relativistic degrees of freedom, energy conservation equations can be solved analytically. The radiation energy density during inflaton φ domination is [35]:

$$\rho_R \propto \begin{cases} a^{-4} & \text{for} \quad a \ll a_{\text{start}}, \\ a^{-\frac{3}{2}} & \text{for} \quad a_{\text{start}} \ll a \ll a_{\text{reh}}, \\ a^{-4} & \text{for} \quad a_{\text{reh}} \ll a, \end{cases} \tag{5.26}$$

where a_{start} and a_{reh} are the scale factors at the start of early matter domination and reheating.

The evolution of temperature is computed from Eq. (3.7):

$$T(a) \propto \begin{cases} a^{-1} & \text{for} \quad a \ll a_{\text{start}}, \\ a^{-\frac{3}{8}} & \text{for} \quad a_{\text{start}} \ll a \ll a_{\text{reh}}, \\ a^{-1} & \text{for} \quad a_{\text{reh}} \ll a. \end{cases} \tag{5.27}$$

Figure 6.5 demonstrated temperature evolution for realistic model inflaton of mass $m_\varphi = 2$ GeV and decay width $T_{\text{reh}} = 40$ MeV.

Version of June 26, 2024 – Created June 27, 2024 - 16:33

Chapter 6

Results

In this section, we numerically solve the equation for transfer function $\mathcal{T}(u)$ in the presence of anisotropic stress (2.14):

$$\mathcal{T}''(u)+2\frac{a'(u)}{a}\mathcal{T}'(u)+\mathcal{T}(u)=-24f_\nu(u)\left(\frac{a'(u)}{a}\right)^2\int_{u_{\rm dec}}^{u}\frac{j_2(u-s)}{(u-s)^2}\mathcal{T}'(s)ds.$$

We explain the method used for solving the equation and present analytic results for different thermal histories of the Universe.

6.1 Numerical solution

To solve Eq.(2.14), we need to know the evolution of scale factor $a(\tau)$ and its derivative $a'(\tau)$ obtained by solving the Friedman equation with the proper energy composition of the Universe. The neutrino fraction in the total energy density $f_\nu(u)$ depends on u through the scale factor as shown in Eq.(B.25). Thus, all the necessary ingredients are determined by $a(\tau)$.

To compute the transfer function with neutrino damping, we must solve the integro-defferential equation, which is a complicated task because the integration must be done over the whole history of the gravitational wave. In addition, the integrand in the right-hand side of the Eq. (2.14) depends on the upper limit of integration, meaning that the integral can not be precomputed, and one must solve the equation for each value of $u=k\tau$ and k [46].

To deal with those problems we used an iterative approach: solve the equation without an integral to obtain $\mathcal{T}^{(0)}(u)$, then treat the integral solutions as corrections. Each $n^{\rm th}$ order correction to $\mathcal{T}^{(n)}(u)$ is the solution of

the Eq. (2.14) with previous correction $\mathcal{T}^{(n-1)}(u)$ in the integral and zero initial conditions:

$$\mathcal{T}(u) = \mathcal{T}^{(0)} + \sum_{n=1}^{N} \mathcal{T}^{(n)} \tag{6.1}$$

$$\mathcal{T}^{(0)}(0) = 1, \qquad \frac{d\mathcal{T}^{(0)}}{d\tau}(0) = 0, \tag{6.2}$$

$$\mathcal{T}^{(n)}(0) = 0, \qquad \frac{d\mathcal{T}^{(n)}}{d\tau}(0) = 0, \qquad n = 1, 2, .., N. \tag{6.3}$$

Here, N denotes the number of performed iterations. This method allows us to precompute the integral and then solve an ordinary differential equation. However, its complexity is $\mathcal{O}(N^2)$ for each mode k. The cycle stops when The correction reaches the required precision. For our purposes, the precision of percent is sufficient, which results in $N \sim 5 - 10$.

In the previous chapter, we demonstrated that solutions of Eq.(2.14) are Bessel functions with oscillatory behavior and rapidly decreasing amplitude, making integration for large u computationally expensive. For high-frequency modes entering the horizon during radiation domination, we integrated up to some large u and matched the result with the WKB approximation [28, 47]:

$$\mathcal{T}(u) = A(u)\sin(u + \delta), \qquad A(u) = \frac{C}{a(u)}, \qquad C = const. \tag{6.4}$$

In our calculations, we solved the equation up to $u_{\text{end}} = 200$, corresponding to ~ 50 oscillations.Since we are only interested in the amplitude $A(u)$, the process can be simplified. To obtain the amplitude, we compute $\mathcal{T}(u)$ and its derivative at the end of the integration, then extract the amplitude and rescale it using $a(\tau)$:

$$A(u) = \sqrt{\mathcal{T}^2(u_{\text{end}}) + \mathcal{T}'^2(u_{\text{end}})}\frac{a_{\text{end}}}{a(u)}. \tag{6.5}$$

Having $\mathcal{T}'(u)$, we insert it into Eq. (4.6) to calculate $\Omega_{GW}(\tau, k)$. The normalization $\Delta^2_{GW,\text{prim}}$ is defined based on the chosen inflation model. For convenience, we use a slow-roll inflationary model, where primordial power spectrum $\Delta^2_{GW,\text{prim}}$ is given by Eq.(D.16).

We used the same calculation parameters as in [28] for comparison. The parameter values are shown in Table 6.1.

First, we checked our numerical routine by comparing our results with those of Watanabe&Komatsu (2006) [28]. The comparison of present-day

Version of June 26, 2024 – Created June 27, 2024 - 16:33

Table 6.1: *Parameters we used for calculations.*

h	0.7
$\Omega_r h^2$	4.15×10^{-5}
$\Omega_m h^2$	$1 - 4.15 \times 10^{-5}$
H_{inf}	2.41×10^{13} GeV
T_0	2.34×10^{-4} eV
$T_{\nu,\text{dec}}$	2 MeV

power spectra $\Omega_{GW}(\tau_0, k)$ for the full frequency kc range is shown in Figure 6.1, while the closer look is given in Figure 6.2. The relatively small differences can be attributed to the details of the implementation of phase transitions and neutrino decoupling. Cavities and peaks in [28] originate from discontinuities in anisotropic stress π_{ij} [37] under the assumption of instantaneous neutrino decoupling [47].

We then examined the PGW spectrum for a model incorporating additional particle content. Since changes in $g_\star$ slightly affect the spectrum, we needed a model with the maximum number of additional degrees of freedom. The supersymmetric extension of the SM, which is known as [2], doubles the effective number of relativistic degrees of freedom at high energies. In this model, each particle is paired with a superpartner based on its spin (bosons have fermionic superpartners, while fermions have bosonic superpartners). Using current constraints on superparticle masses [2], we set their freeze-out temperature at approximately 10 TeV. Figure 6.3 shows, that this transition results in the slight ($\sim$ 20%) damping at k corresponding to supersymmetry breaking.

Nevertheless, varying $g_\star$ does not create a significant suppression of the spectrum. To get a notable effect, we shall look at EMD scenarios.

6.2 Results for early matter domination

In the early matter domination model described in Section 5.2, we have three parameters: the scalar field φ mass m_φ, its decay width Γ_φ, and its relative contribution to the energy budget of the Universe ρ_φ/ρ_R.

To calculate the scale factor, we solved the coupled Boltzmann equations (5.20) and (5.21), using variables that change slowly with the scale factor a: $R = \rho_R a^4$ and $\Phi = \rho_\varphi a^4$. Additionally, we used a logarithmic scale for better efficiency. Initial conditions were set to match the observed present radiation energy density $\rho_R = \pi^2 g_\star(T_{\text{CMB}}) T_{\text{CMB}}^4/30$. Initially, we

Version of June 26, 2024 – Created June 27, 2024 - 16:33

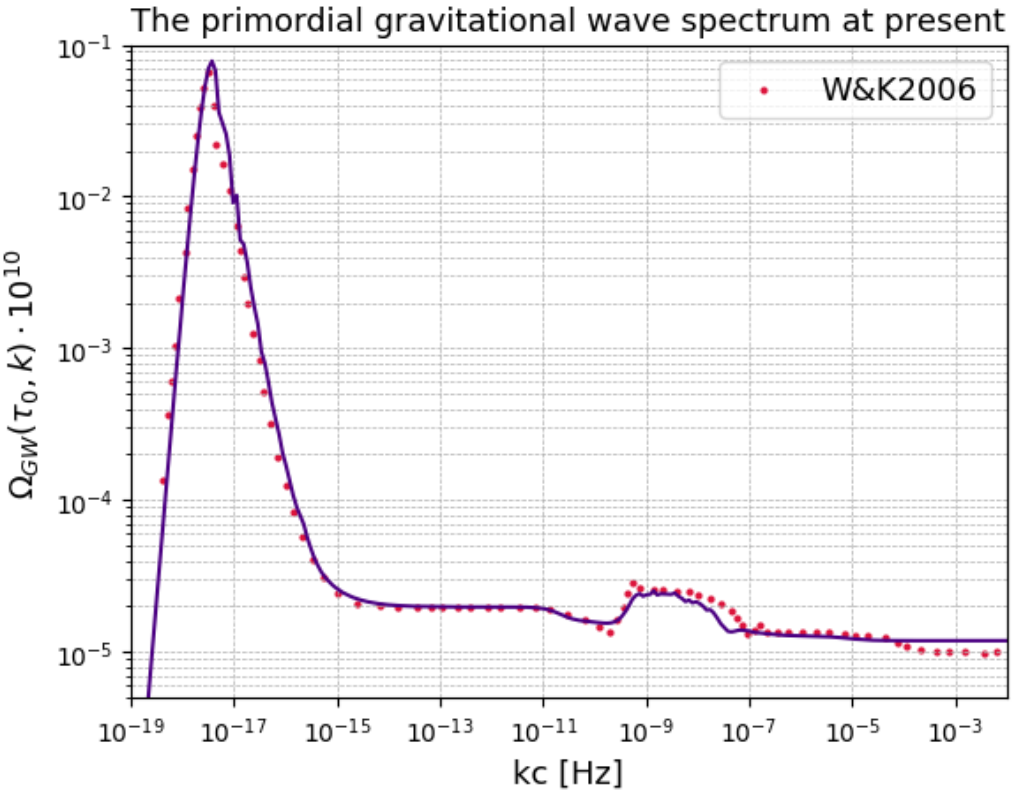

Figure 6.1: *Spectrum of primordial gravitational waves at $\tau = \tau_0$ as the function of comoving wavelength k (frequency kc in Hz). The solid line represents our numerical solution, while dots are the results of Watanabe&Komatsu (2006) [28].*

assumed that after reheating, the radiation energy density primarily originated from the φ field energy: $R(a_{\rm reh}) = \Phi(a_{\rm EMD})a_{\rm reh}/a_{\rm EMD}$, where $a_{\rm reh}$ is the scale factor at the end of reheating and $a_{\rm EMD}$ is the scale factor when φ becomes non-relativistic. Here, we interchangeably use EMD and *freeze-out* (the moment when φ becomes non-relativistic) defining it as when the Universe's equation of state deviates from radiation. We solved the Boltzmann equations, rescaled the results to match the observed present values at $a_0 = 1$, and then solved these equations again with proper initial conditions. Figure 6.4 shows ρa^4 for a scenario with specified m_φ and Γ_φ. Figure 6.5 represents temperature T as a function of scale factor a for the same model.

With the evolution of all energy components as functions of a, we calculated the scale factor time dependency $a(\tau)$ using the Friedmann equation (5.22). This allowed us to generate the PGW spectrum using the algo-

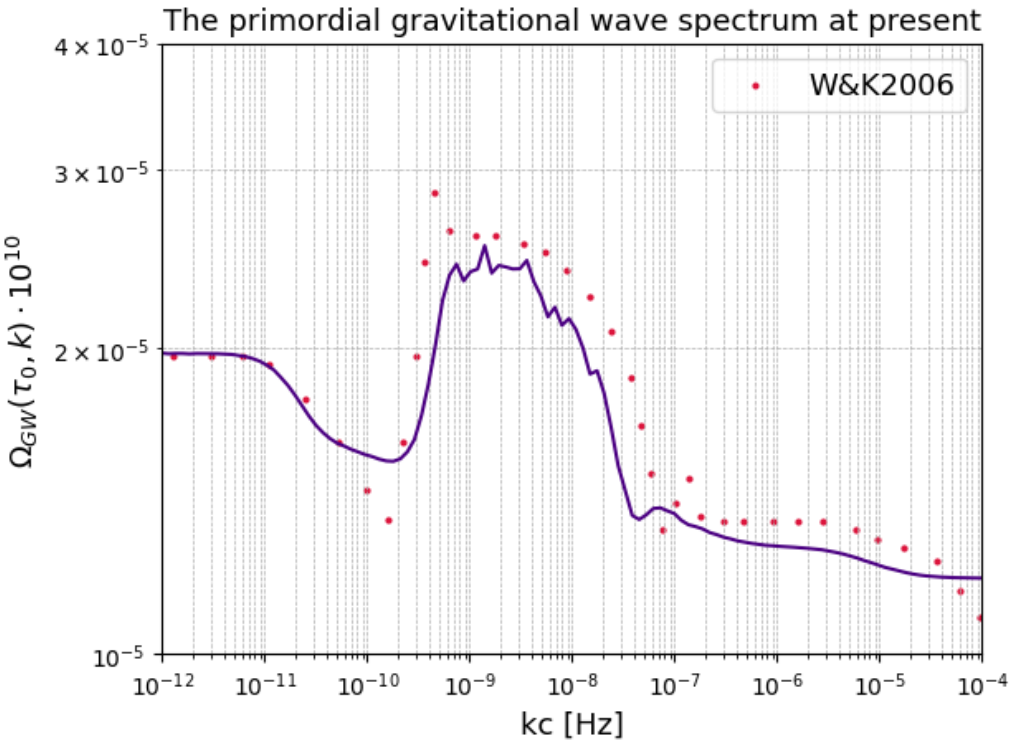

Figure 6.2: *Zoomed-in part of PGWspectrum from Figure 6.1, featuring key transitions during radiation domination. The solid line represents our numerical solution, while dots are the results of Watanabe&Komatsu (2006) [28].*

rithm from the previous section. The result is shown in Figure 6.6.

We first considered unstable massive particles φ constituted 1% of the total energy budget of the Universe before becoming non-relativistic. This assumption is based on $g_\star$: the total $g_\star \sim 100$ at $T \gtrsim 10^2$ MeV, with new physics particles contributing approximately $g_\varphi \sim 1$ degree of freedom.

Figure 6.7 shows the PGWspectrum for particles with various masses and reheating temperature $T_{\text{reh}} = 1$ GeV. Figure 6.8 depicts the PGWspectrum for particles with a mass of $m_\varphi = 10^6$ GeV and different decay widths. We also varied the initial (right after inflation) $\frac{R}{\Phi} = \frac{\rho_R}{\rho_\varphi}$ ratio while keeping $m_\varphi = 10^2$ GeV and $T_{\text{reh}} = 1$ GeV constant. These results are shown in Figure 6.9.

All plots exhibit a distinct step-like feature caused by the energy transfer from the φ field to radiation. This property appears in all models with massive unstable particles, regardless of whether they dominate the energy density of the Universe. The width and height of the step depend on

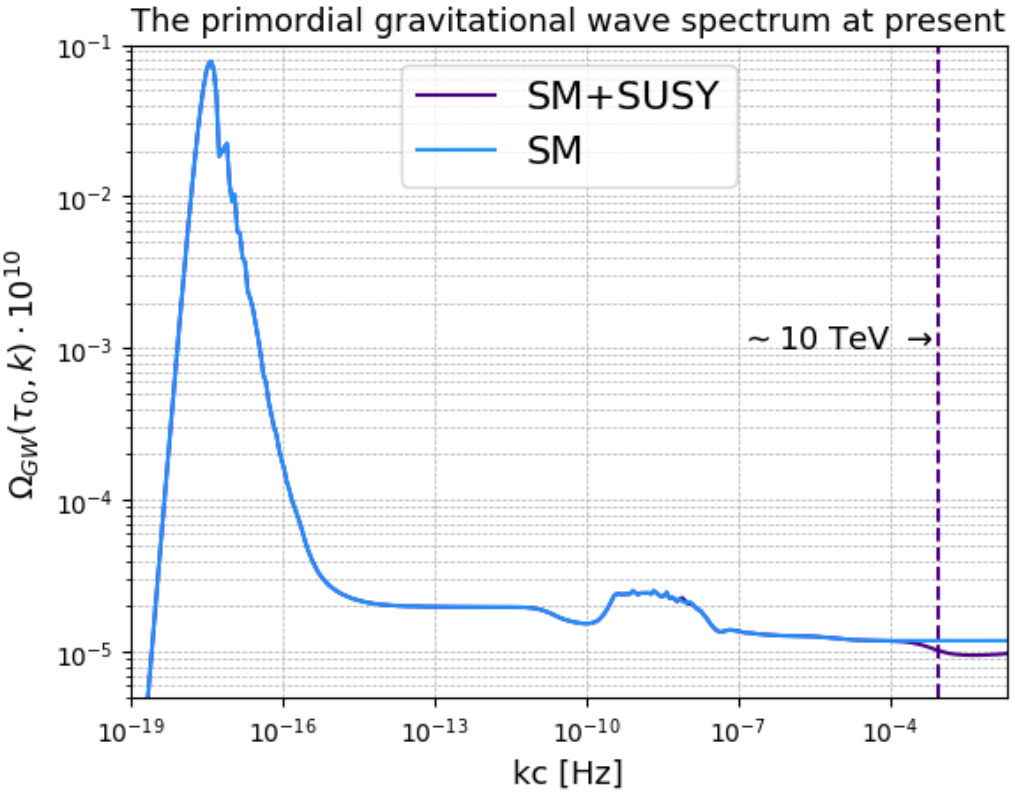

Figure 6.3: *Spectrum of primordial gravitational waves at $\tau = \tau_0$ as the function of comoving wavelength k (frequency kc in Hz). The solid blue line represents our numerical solution for SM particle content, while the indigo line also accounts for SUSY particles. The dashed vertical line marks the SUSY phase transition at $T \sim 10$ TeV.*

m_φ, Γ_φ, and $\frac{\rho_R}{\rho_\varphi}$ and can be expressed analytically.

To get the influence of the mass of the φ on the suppression, we fixed Γ_φ and used the definition of $\Omega_{GW}(\tau, k)$ and energy density evolution laws. As a result, we get:

$$\Omega_{GW}(\tau, k) = \frac{\tilde{\rho}_{GW}(\tau, k)}{\rho_{\text{cr}}(\tau)} \propto \frac{a^{-4}}{\rho_m(a)} \propto \frac{1\,\text{GeV}}{m_\varphi} a^{-1} \tag{6.6}$$

during matter domination. This means suppression is inversely proportional to m_φ. The heavier the φ component, the faster the expansion of the Universe and the greater the damping effect. In addition, m_φ unequivo-

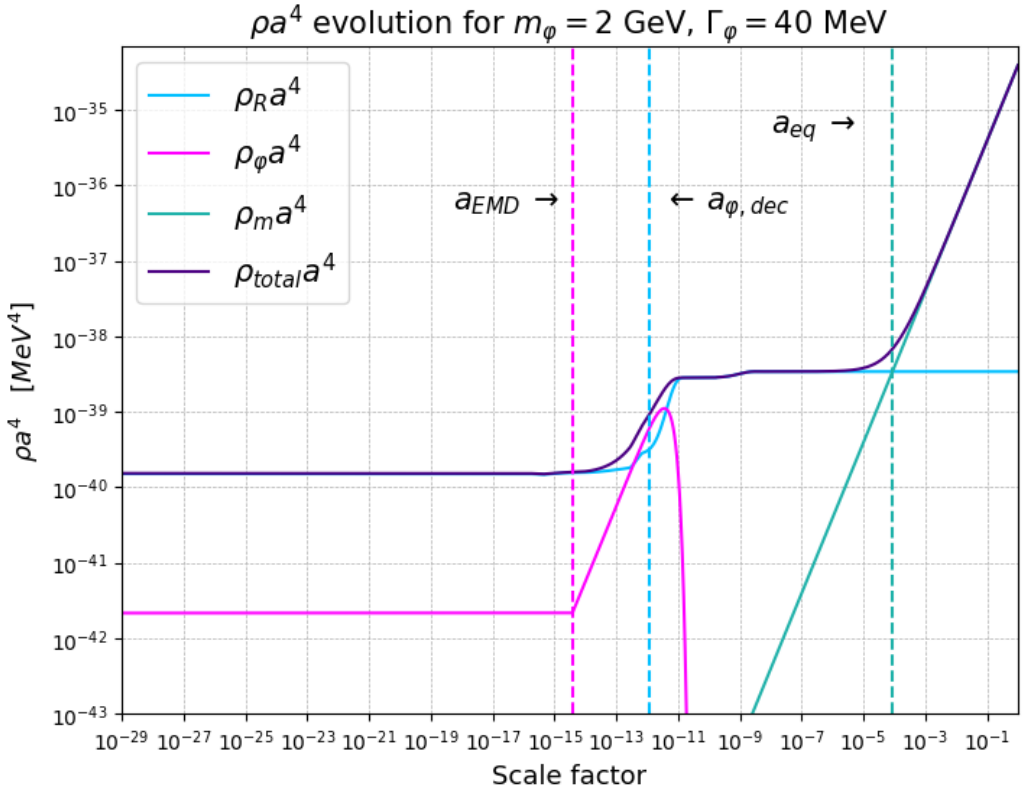

Figure 6.4: *Evolution of the energy density ρa^4 as a function of the scale factor in a model with EMD induced by $m_\varphi = 2$ GeV particle with decay width $T_{\rm reh} = 40$ MeV. Solid lines represent radiation (blue), φ (magenta), matter (green), and the total energy density of the Universe (indigo). Dashed vertical lines indicate transitions to EMD (magenta), reheating (blue), and MD (green).*

cally determines the beginning of EMD, in terms of wavelength:

$$k_{\rm EMD} \propto a_{\rm EMD}^{-1/2} \propto \left(\frac{T_{\rm EMD}}{T_{\rm r}}\right)^{1/2} \propto \left(\frac{m_\varphi}{T_{\rm r}}\right)^{1/2}, \tag{6.7}$$

where $T_{\rm r}$ is some reference temperature from the early radiation domination. However, $k_{\rm EMD}$ can be calculated using only the characteristics of φ, as they are the only dimensional parameters in the model.

Figure 6.7 supports our conclusions.

Decay width Γ_φ controls the reheating temperature, as $T_{\rm reh} \propto \sqrt{\Gamma_\varphi M_{Pl}}$, neglecting the change in $\gamma_\star$. Fixing the mass m_φ and using the temperature

Version of June 26, 2024 – Created June 27, 2024 - 16:33

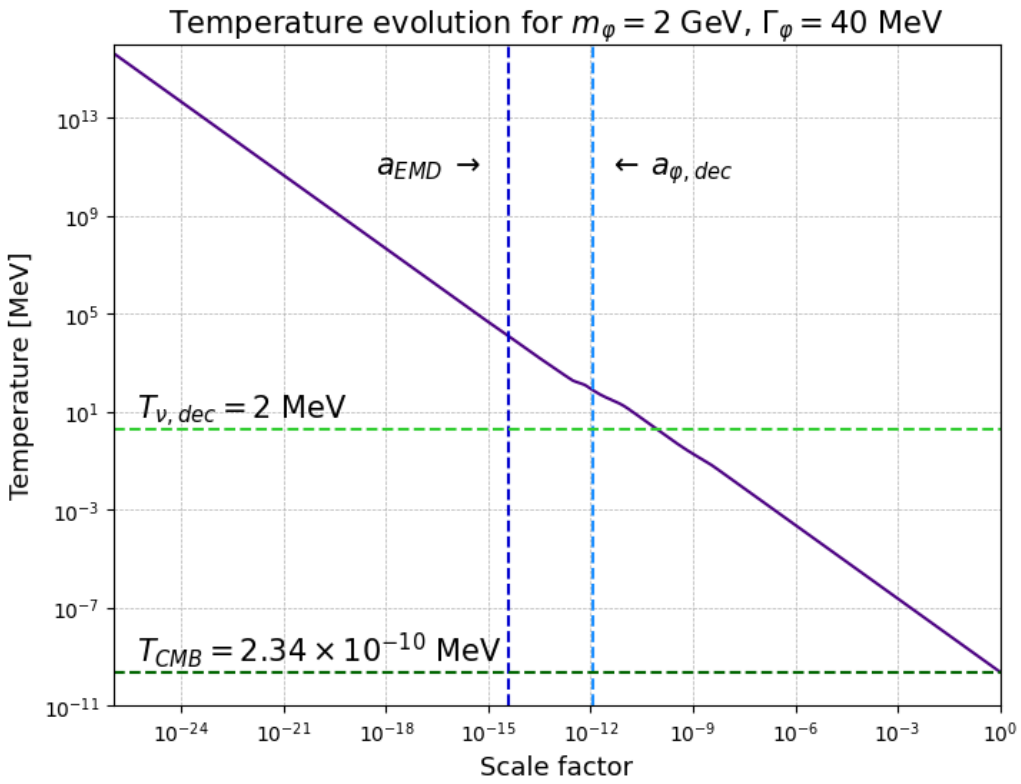

Figure 6.5: *Temperature evolution as a function of scale factor in a model with EMD induced by $m_\varphi = 2$ GeV particle with decay width $T_{reh} = 40$ MeV. Dashed vertical lines mark start of EMD a_{EMD} and reheating $a_{\varphi,dec}$. Dashed horizontal lines represent the temperatures at neutrino $T_{\nu,dec} = 2$ MeV and the present CMB temperature $T_{CMB} = 2.34 \cdot 10^{-10}$ MeV.*

evolution during RD and EMD (5.27), we find:

$$k_{\text{reh}} = \frac{\tau_0}{\tau_{\text{reh}}} k_0 = \frac{a_0}{a_{\text{reh}}} k_0 = \frac{T_{\text{reh}}}{T_0} k_0 = C(T_{\text{reh}}) \frac{\sqrt{\Gamma_\varphi M_{Pl}}}{T_0} k_0, \tag{6.8}$$

$$k_{\text{EMD}} = \frac{\tau_{\text{reh}}}{\tau_{\text{EMD}}} k_{\text{reh}} = \left(\frac{a_{\text{reh}}}{a_{\text{EMD}}}\right)^{1/2} k_{\text{reh}} = \frac{T_{\text{EMD}}^{4/3}}{T_{\text{reh}}^{1/3} T_0} k_0 = \frac{C^{-1/3}(T_{\text{reh}}) m_\varphi^{4/3}}{\Gamma_\varphi^{1/6} M_{Pl}^{1/6} T_0} k_0, \tag{6.9}$$

where $T_0 = T_{\text{CMB}}$ and $k_0 = \tau_0^{-1}$ are the present day values, and

$$C(T_{\text{reh}}) = \left(\frac{45}{4\pi^3 g_\star(T_{\text{reh}})}\right)^{1/4}.$$

Therefore, a larger decay width results in earlier reheating. Figure 6.8 illustrates this statement. Shifts in the beginning of the EMD can be attributed

Version of June 26, 2024 – Created June 27, 2024 - 16:33

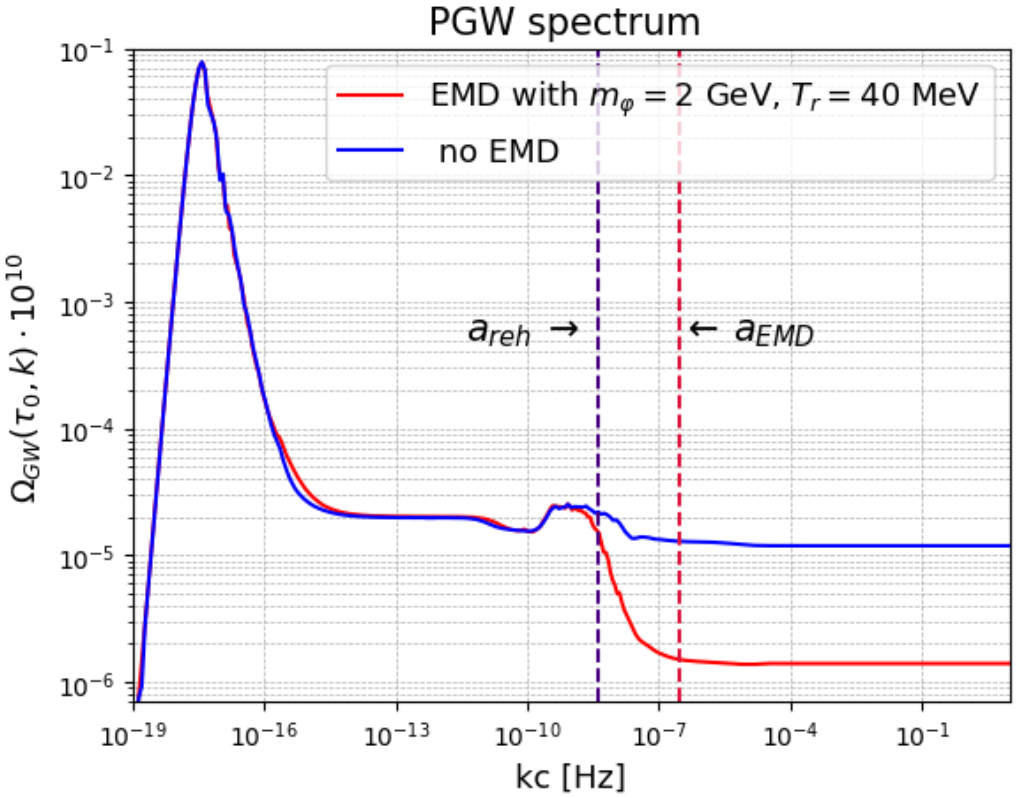

Figure 6.6: *Spectrum of primordial gravitational waves at $\tau = \tau_0$ as the function of comoving wavelength k (frequency kc in Hz). The blue line corresponds to the conventional radiation domination, while the red line describes the scenario with EMD induced by $m_\varphi = 2$ GeV particle with reheating temperature $T_{reh} = 40$ MeV. Dashed vertical lines mark the start of the EMD (red) and reheating (blue).*

to changes in initial conditions due to rescaling to match the observed radiation energy density.

The magnitude of suppression μ can be expressed as a function of both m_φ and Γ_φ:

$$\boxed{\mu = \frac{\Omega_{GW}^{\mathrm{EMD}}}{\Omega_{GW}^{\mathrm{reh}}} = \frac{a_{\mathrm{reh}}}{a_{\mathrm{EMD}}} = \left(\frac{m_\varphi^2}{\Gamma_\varphi M_{Pl}}\right)^{2/3}}. \tag{6.10}$$

Hence, the longer particles live (smaller decay width) and the higher their masses, the greater suppression is.

In the calculation above, we assumed that particles φ constitute $\sim 1\%$ of the initial energy density as a realistic scenario. However, we varied this parameter as well. Figure 6.9 shows results for different initial

Version of June 26, 2024 – Created June 27, 2024 - 16:33

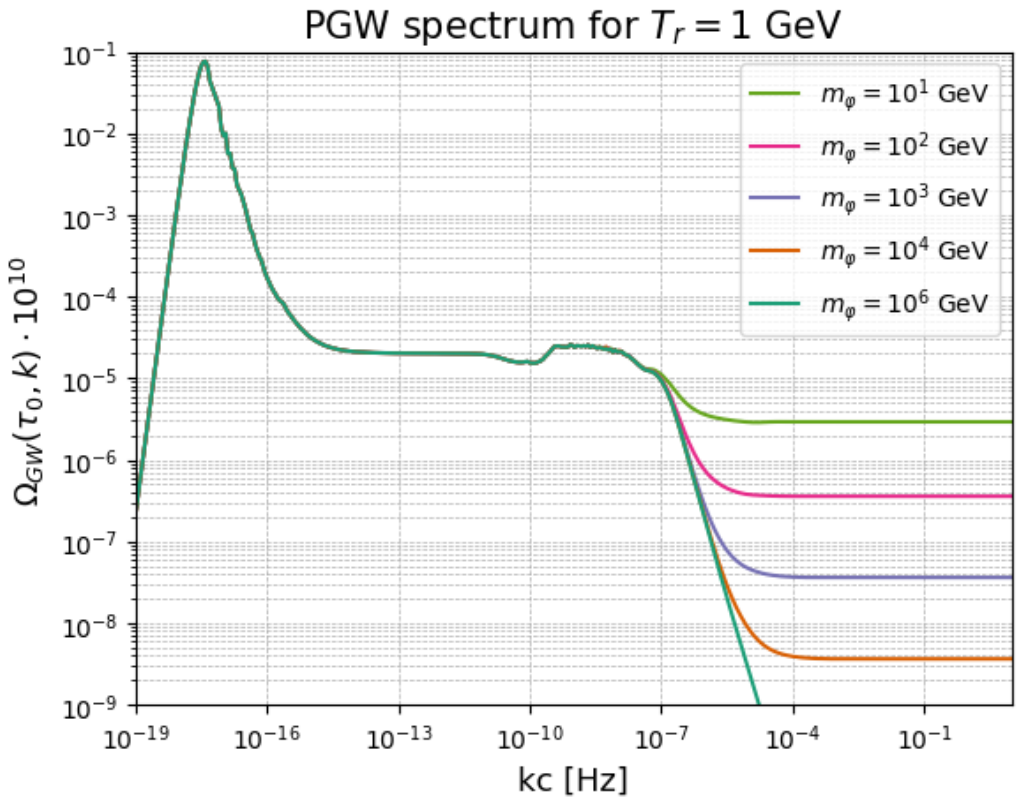

Figure 6.7: *Spectra of primordial gravitational waves at $\tau = \tau_0$ as functions of comoving wavelength k (frequency kc in Hz). Different colors (green, magenta, violet, orange, seagreen) represent scenarios with EMD induced by particles of varying masses: 10^1 GeV, 10^2 GeV, 10^3 GeV, 10^4 GeV, and 10^6 GeV, all with a reheating temperature $T_{reh} = 1$ GeV.*

$R/\Phi = \Omega_r^{\text{init}}/\Omega_\varphi^{\text{init}}$ ratios, where φ is always subdominant. A more precise expression for the beginning of EMD, which accounts for the energy distribution between φ and radiation, is:

$$a_{\text{EMD}}^{\text{precise}} = \frac{\Omega_r^{\text{init}}}{\Omega_\varphi^{\text{init}}} a_{\text{freeze-out}}\,, \tag{6.11}$$

where $a_{\text{freeze-out}}$ is the scale factor at freeze-out. The smaller the energy fraction of the φ field, the later it starts to dominate. For fixed m_φ and Γ_φ, the suppression is $\propto \Omega_r^{\text{init}}/\Omega_\varphi^{\text{init}}$. Interestingly, this ratio impacts $\Omega_{GW}(\tau_0, k)$ as m_φ, that generalizes as the influence on ρ_{cr}.

As a result, measuring the magnitude of the suppression and EMD duration could facilitate inferring the mass and decay width of particles caus-

Version of June 26, 2024 – Created June 27, 2024 - 16:33

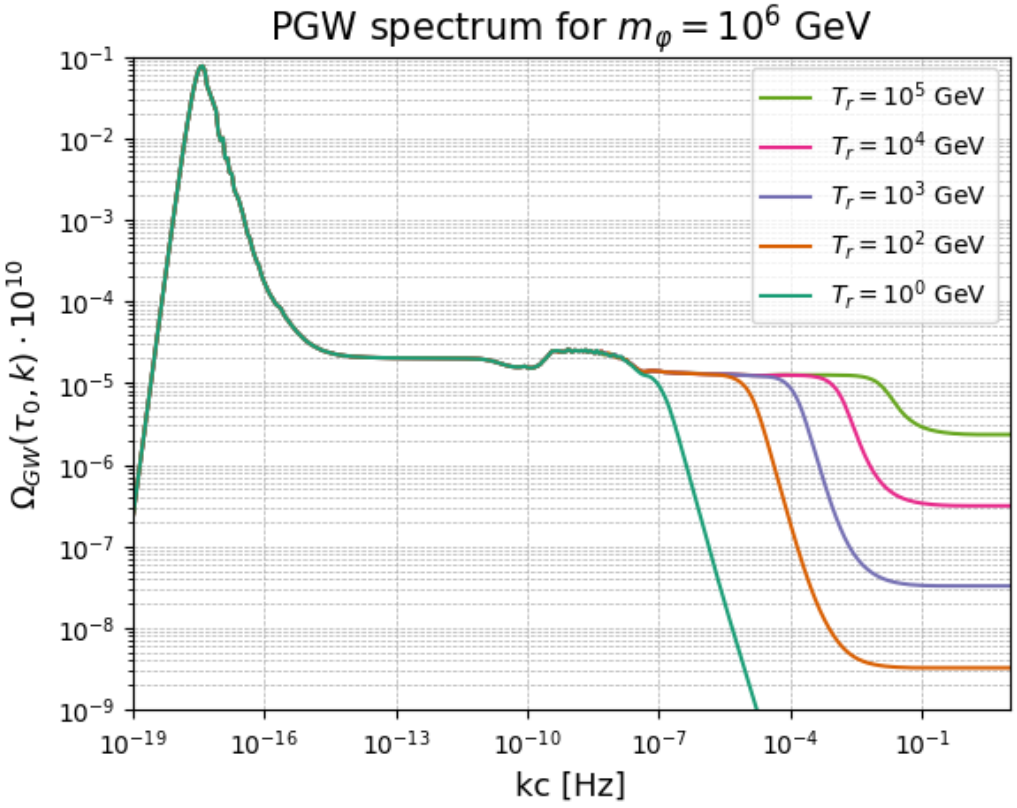

Figure 6.8: *Spectra of primordial gravitational waves at $\tau = \tau_0$ as functions of comoving wavelength k (frequency kc in Hz). Different colors (green, magenta, violet, orange, seagreen) represent scenarios with EMD induced by particles of varying reheating temperatures: 10^0 GeV, 10^2 GeV, 10^3 GeV, 10^4 GeV, and 10^5 GeV, all with a mass $m_\varphi = 10^6$ GeV.*

ing EMD, potentially excluding some new physics particles (e.g., heavy neutral leptons) unreachable by current and proposed collider experiments.

Heavy neutral leptons

One attractive beyond Standard Model scenario is the minimal standard electroweak gauge model with heavy neutral leptons (HNLs) [48, 49]. These particles are the right-handed partners of SM neutrinos, characterized by a Dirac mass matrix m_N and a matrix of mixing angles between HNLs and SM neutrinos U_α, where $\alpha = e, \mu\, \tau$ denotes the flavor of active neutrinos, and N denotes the HNL.

The decay width can be expressed in terms of mixing angles and masses

Version of June 26, 2024 – Created June 27, 2024 - 16:33

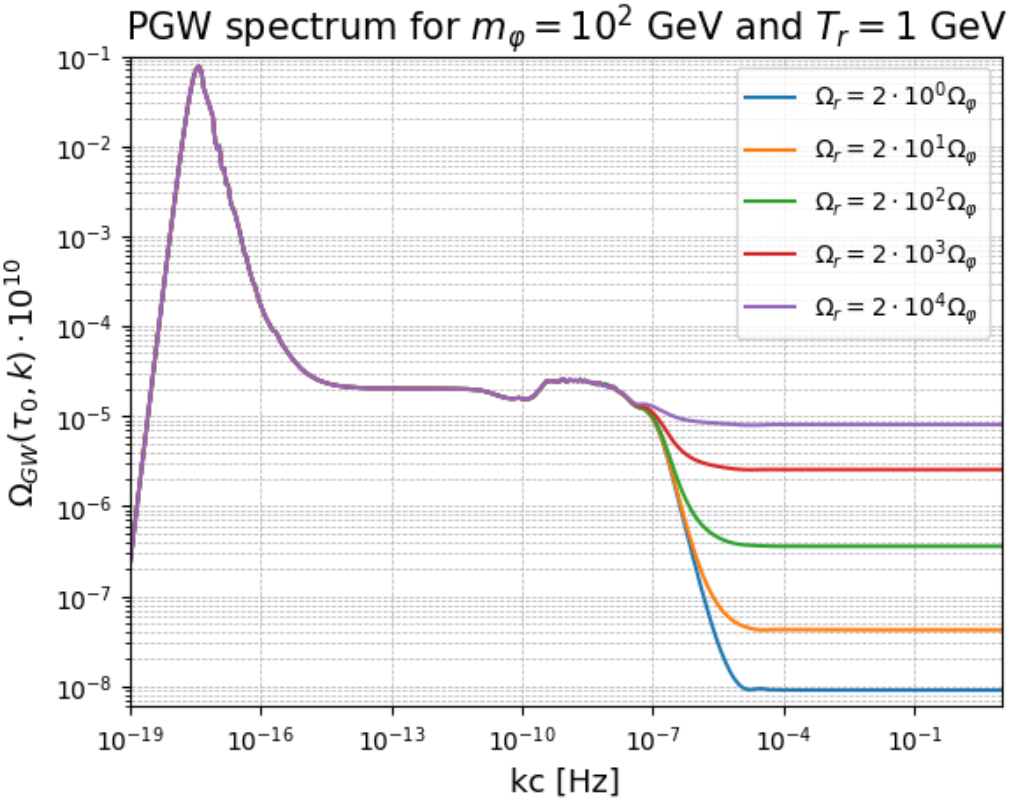

Figure 6.9: *Spectra of primordial gravitational waves at $\tau = \tau_0$ as functions of comoving wavelength k (frequency kc in Hz). Different colors (green, magenta, violet, orange, seagreen) represent scenarios with EMD induced by particles with a mass $m_\varphi = 100$ GeV, reheating temperature $T_{reh} = 1$ GeV, and varying initial radiation-to-φ ratios: $\Omega_r = 2 \cdot 10^0 \Omega_\varphi$, $\Omega_r = 2 \cdot 10^1 \Omega_\varphi$, $\Omega_r = 2 \cdot 10^2 \Omega_\varphi$, $\Omega_r = 2 \cdot 10^3 \Omega_\varphi$, and $\Omega_r = 2 \cdot 10^4 \Omega_\varphi$.*

as [50]:

$$\Gamma \approx U^2 \frac{G_F^2 m_N^5}{192\pi^3} \sim 10^{-21}\,\text{MeV} \frac{m_\nu}{0.05\,\text{eV}} \left[\frac{m_N}{1\,\text{GeV}}\right]^4. \tag{6.12}$$

A crucial aspect of models with HNLs is the seesaw mechanism, where an effective dimension-five operator produces neutrino masses [51]. The following equations describe this mechanism:

$$U = m_N M_M^{-1}, \qquad m_\nu = U M_M U^T, \qquad U^2 \approx \frac{m_\nu}{m_N}, \tag{6.13}$$

where M_M is the Majorana mass matrix for HNLs, and m_ν is the SM neutrino mass. The increase in Majorana masses M_M leads to the growth of

SM neutrino masses and a decrease of HNL masses like they are on a seesaw.

In this framework, the minimal value of mixing angles is called *the seesaw limit* U_{seesaw}:

$$U_{\text{seesaw}} \sim \frac{\sqrt{\Delta m^2_{\text{atm.}}}}{m_N}, \tag{6.14}$$

where $\Delta m^2_{\text{atm.}} = 50\,\text{meV}^2$ is the mass scale of the active neutrinos. HNLs with smaller mixing angles cannot generate neutrino masses, providing strong constraints on the HNL parameter space.

PGW spectrum can validate or exclude HNL models. By deducing Γ_α and m_N from the spectrum damping characteristics, we can compute U_α. If this value is smaller than the seesaw limit, the particle responsible for the phenomenon is not an HNL. Conversely, if the step-like feature predicted by an HNL model is absent in the PGW spectrum, the model can be excluded. If the predicted damping is observed, it can be attributed to this scenario, hinting at new physics.

Figures 6.4, 6.5, and 6.6 demonstrate energy density evolution, temperature evolution, and PGW spectrum for a realistic model of a 2 GeV HNL at the seesaw limit, with a reheating temperature of 40 MeV. In this scenario, the damping is about $\sim 90\%$.

Version of June 26, 2024 – Created June 27, 2024 - 16:33

Chapter 7

Conclusions

Primordial gravitational waves, predicted by any inflation model, are the promising frontier in cosmology for probing the earliest stages of the Universe and physics at energies far beyond the capabilities of current collider experiments. Detecting this nearly scale-invariant stochastic gravitational wave background would validate the inflationary paradigm and provide unique insights into the processes occurring before BBN. Recent advancements in gravitational wave detection technology have made this topic more relevant.

Due to their weak coupling with matter, primordial GWs propagate through spacetime with minimal distortion, preserving precious information about their origins. However, changes in the effective number of relativistic degrees of freedom and neutrino free-streaming leave imprints on the PGW spectrum. For example, a damping effect neutrino anisotropic stress causes 35% damping. By analyzing these features, we can infer details about the thermal history of the Universe and put constrain physics beyond the Standard Model (e.g., properties of heavy neutral leptons).

In this thesis, we focused on non-standard thermal histories of the Universe, particularly scenarios with early matter domination induced by unstable long-lived massive particles φ. By examining the imprints of these epochs left on the PGW spectrum, we aimed to distinguish between various cosmological models. We accomplished this task by numerically solving the gravitational wave equation in the presence of anisotropic stress and analyzing its solutions in the form of power spectrum $\Omega_{GW}(\tau_0, k)$.

Our main results indicate that the spectrum of primordial gravitational waves receives a step-like feature as a result of the EMD. This feature is highly sensitive to the parameters of the EMD model: the mass m_φ, decay width Γ_φ, and the fraction in the energy density of the field φ. Changes in

Version of June 26, 2024 – Created June 27, 2024 - 16:33

these parameters create distinct signatures in the PGW spectrum, which allows us to put constraints on the properties of these particles φ.

The extent of the suppression of the spectrum of primordial gravitational waves is inversely proportional to the mass of the field as $m_\varphi^{-4/3}$ and directly proportional to the decay width as $\propto \Gamma_\varphi^{2/3}$. In addition, the damping is also inversely proportional to the initial fraction of energy density of φ relative to that of the radiation $\Omega_\varphi^{\text{init}}/\Omega_r^{\text{init}}$. Heavier and more dominant particles cause a faster expansion of the Universe, which increases the damping effect. The shorter the lifetime of φ is, the less they affect the power spectrum.

Moreover, we related model parameters to the scale factors a and frequency kc at the key transitions – the beginning of the EMD and reheating. We provided the precise expressions corrected for the time required to reach EMD from the freeze-out.

In addition, we considered a specific model of particles φ – heavy neutral leptons. The analysis showed that there is a potential to constrain HNL models by studying the properties of the PGW spectrum at high frequencies. The presence or absence of specific features in the PGW spectrum can validate or exclude certain HNL scenarios. This issue required further investigation.

To conclude, primordial gravitational waves have a complex connection to the thermal history of the Universe. Exploration of the properties of their power spectrum could provide unique information about the early Universe and offer hints for New Physics.

Acknowledgements

I would like to express my gratitude to my supervisor, Dr. Subodh Patil, for his support and encouragement during this research. In addition, I would like to thank Alex Mikulenko for fruitful discussions.

Appendices

Appendix A

Bessel Functions

This appendix presents expressions for spherical Bessel functions and their properties. Each Bessel function $z_n(x)$ satisfies following differential equations:

$$\frac{d}{dx}\left[\frac{z_n(x)}{x^n}\right] = -\frac{z_{n+1}(x)}{x^n}, \tag{A.1}$$

$$\frac{d}{dx}\left[x^{n+1} z_n(x)\right] = x^{n+1} z_{n-1}(x). \tag{A.2}$$

Bessel functions can be redefined in terms of basic trigonometric functions:

$$j_0(x) = \frac{\sin x}{x}, \tag{A.3}$$

$$j_1(x) = \frac{\sin x}{x^2} - \frac{\cos x}{x}, \tag{A.4}$$

$$j_2(x) = \frac{1}{x}\left(\frac{3}{x^2} - 1\right)\sin x - \frac{3}{x^2}\cos x, \tag{A.5}$$

$$y_0(x) = -\frac{\cos x}{x}, \tag{A.6}$$

$$y_1(x) = -\frac{1}{x}\left(\frac{1}{x}\cos x + \sin x\right), \tag{A.7}$$

$$y_2(x) = -\frac{1}{x}\left(\frac{3}{x^2} - 1\right)\cos x - \frac{3}{x}\sin x, \tag{A.8}$$

$$h_1^{(1)}(x) = -\frac{1}{x}\left(1 + \frac{i}{x}\right)e^{-ix}, \tag{A.9}$$

$$h_1^{(2)}(x) = -\frac{1}{x}\left(1 - \frac{i}{x}\right)e^{-ix}. \tag{A.10}$$

The connection between spherical Bessel $j_n(x)$ and Neumann $y_n(x)$ functions is:

$$y_n(x) = (-1)^{n+1} j_{-n-1}(x). \tag{A.11}$$

The approximations For large arguments $x \gg 1$ are:

$$j_n(x) \approx \frac{\sin(x - n\pi/2)}{x}, \quad y_n(x) \approx -\frac{\cos(x - n\pi/2)}{x}. \tag{A.12}$$

Version of June 26, 2024 – Created June 27, 2024 - 16:33

Appendix B

Neutrino free-streaming

In this appendix, we present the derivation of the equation for the transfer function $\mathcal{T}(\tau, k)$, which accounts for the anisotropic stress tensor π_{ij} due to neutrino free-streaming. Our derivation follows the approach outlined by Weinberg, 2004 [16] and Watanabe et al., 2006 [28].

We begin by introducing the desired quantity, the anisotropic stress tensor π_{ij}. In a curved space, the amplitude and stress-energy tensor for perturbations are given by

$$h_{ij}(\tau, \mathbf{x}) = \sum_{\lambda=+,\times} \int \frac{d^3k}{(2\pi)^3} h_\lambda(\tau, \mathbf{k}) e^{i\mathbf{k}\cdot\mathbf{x}} \epsilon^\lambda_{ij}(\mathbf{x}), \tag{B.1}$$

$$\delta T^\nu_{ij} = a^2 \sum_{\lambda=+,\times} \int \frac{d^3k}{(2\pi)^3} \pi_{\lambda,\mathbf{k}} e^{i\mathbf{k}\cdot\mathbf{x}} \epsilon^\lambda_{ij}(\mathbf{x}), \tag{B.2}$$

where $\epsilon^\lambda_{ij}(\mathbf{x})$ are tensor harmonics that depend on the spatial coordinate $\mathbf{x}$. These quantities satisfy the Helmholtz equation:

$$\epsilon^\lambda_{ij|a}{}^{|a}(\mathbf{x}) + k^2 \epsilon^\lambda_{ij}(\mathbf{x}) = 0, \qquad \partial_\alpha \epsilon^\lambda_{ij} = i k_l \epsilon^\lambda_{ij}, \tag{B.3}$$

and have the following properties:

$$\epsilon^\lambda_{ij}(\mathbf{x}) = \epsilon^\lambda_{ji}(\mathbf{x}), \qquad \epsilon^{\lambda\,|j}_{ij} = a^2 \bar{g}^{ij} \epsilon^\lambda_{ij} = 0, \tag{B.4}$$

where $|$ denotes the covariant derivative with respect to the unperturbed metric $\gamma^{ij} = a^2 \bar{g}^{ij}$.

Version of June 26, 2024 – Created June 27, 2024 - 16:33

To calculate perturbations in the neutrino distribution function, we must determine its exact form. For neutrinos after decoupling, the distribution function $f(\mathbf{x}, \mathbf{p}, t)$ satisfies the Vlasov equation:

$$\frac{df(\mathbf{x}, \mathbf{p}, t)}{dt} = \frac{\partial f}{\partial t} + \frac{dx^i}{dt}\frac{\partial f}{\partial x^i} + \frac{dp^i}{dt}\frac{\partial f}{\partial p^i} = 0, \tag{B.5}$$

$$f_0(p_0) = \frac{g_\nu}{e^{p_0/T} + 1}, \qquad f(\mathbf{x}, \mathbf{p}, t) = f_0(\mathbf{x}, \mathbf{p}) + \delta f(\mathbf{x}, \mathbf{p}, t), \tag{B.6}$$

where $f_0(p_0)$ is the equilibrium distribution function, while $\delta f(\mathbf{x}, \mathbf{p}, t)$ accounts for perturbations. The real time is denoted by t, and g_ν represents the number of possible spin projections for neutrinos. We neglect neutrino masses and treat them as photons:

$$p^\alpha = \frac{d}{ds}x^\alpha, \qquad g_{\alpha\beta}p^\alpha p^\beta = 0, \qquad p^0 = \sqrt{g_{ij}p^i p^j}. \tag{B.7}$$

The derivative $\frac{\partial f}{\partial x^i}$ is linear in perturbation (since (f_0 depends only on p^α), implying that $\frac{dx^i}{dt}$ must be unperturbed:

$$\frac{dx^i}{dt} = \frac{dx^i}{ds}\frac{ds}{dt} = \frac{p^i}{p^0}. \tag{B.8}$$

The last term in the Vlasov equation is more complicated. Its first factor is given by:

$$\frac{dp^i}{dt} = \frac{dp^i}{ds}\frac{ds}{dt} = -\Gamma^i_{jk}\frac{p^j p^k}{p^0} = \frac{p^j p^k}{2p^0}\frac{\partial g_{jk}}{\partial x^i}, \tag{B.9}$$

where we have used the geodesic equation and the expression for Christoffel symbols:

$$\Gamma^i_{jk} = \frac{g^{il}}{2}\left(\frac{\partial g_{jl}}{\partial x^k} + \frac{\partial g_{kl}}{\partial x^j} - \frac{\partial g_{jk}}{\partial x^l}\right), \tag{B.10}$$

and $g_{00} = -1$, $g_{0i} = 0$.

To understand the interaction between gravitational waves and neutrinos, we examine the energy component associated with neutrinos:

$$\frac{dp^0}{dt}\frac{1}{p^0} = -\Gamma^0_{jk}\frac{p^j p^k}{(p^0)^2} = -\frac{a'}{a} - a^2\frac{p^j p^k}{2(p^0)^2}\frac{\partial h_{jk}}{\partial t}. \tag{B.11}$$

The first term represents energy loss due to the expansion of the Universe. The second term describes the interaction between gravitational waves

Version of June 26, 2024 – Created June 27, 2024 - 16:33

and neutrinos. Depending on the sign of $\frac{\partial h_{jk}}{\partial t}$, neutrinos either give or receive energy from the wave. This effect manifests as damping or enhancement. Particularly, for massive particles, the last term is proportional to velocity squared v^2, implying that massive neutrinos are less affected by gravitational waves.

Now, we express the Vlasov equation in a simplified form. Using appropriate transformations, we obtain:

$$\frac{\partial f}{\partial t} + \frac{\partial f}{\partial x^i}\frac{p^i}{p^0} + \frac{\partial f}{\partial p^i}\frac{p^j p^k}{2p^0}\frac{\partial g_{jk}}{\partial x^i} = 0. \tag{B.12}$$

In the linear order of perturbations, Eq.(B.12) becomes:

$$\frac{\partial \delta f(\mathbf{x},\mathbf{p},t)}{\partial t} + \frac{\partial \delta f(\mathbf{x},\mathbf{p},t)}{\partial x^i}\frac{\hat{p}_i}{a(t)} = \tag{B.13}$$
$$= -\frac{p}{2a(t)}\frac{\partial f_0(P)}{\partial P}\hat{p}_i\hat{p}_j\hat{p}_k\frac{\partial}{\partial x^k}\big(h_{ij}(\mathbf{x},t) - h_{ij}(\mathbf{x},t_{\rm dec})\big).$$

Here, we have used $p^i = a^{-2}p_i$, $p^0 = a^{-1}\sqrt{p_i p_i} = a^{-1}p$, $p_i = \hat{p}_i p$, and expanded the distribution function $f_0(\mathbf{x},\mathbf{p})$ into Taylor series:

$$f_0(\mathbf{x},\mathbf{p}) = f_0(P) - \frac{1}{2}\frac{\partial f_0(P)}{\partial P}h_{ij}(\mathbf{x},t)\frac{p^i p^j}{p}, \tag{B.14}$$

where $P = p\cdot a$.

When neutrinos decouple at $t = t_{\rm dec}$, their distribution function remains unperturbed $\delta f = 0$. We can find the solution to Eq.(B.13) using Fourier transformation:

$$f_{\mathbf{k}}(\mathbf{p},u) = e^{-i\hat{p}\cdot\hat{k}(u-u_{\rm dec})}f_{\mathbf{k}}(\mathbf{p},u_{\rm dec}) - \frac{i}{2}p\frac{\partial f_0(P)}{\partial P}(\hat{p}\cdot\hat{k})\hat{p}_i\hat{p}_j \tag{B.15}$$
$$\times\int_{u_{\rm dec}}^{u} ds e^{-i\hat{p}\cdot\hat{k}(s-u)}\big(h_{ij}(s) - h_{ij}(u_{\rm dec})\big).$$

The resulting distribution function is then given by:

$$f_{\mathbf{k}}(\mathbf{p},u) = e^{-i\hat{p}\cdot\hat{k}(u-u_{\rm dec})}f_{\mathbf{k}}(\mathbf{p},u_{\rm dec}) + \frac{p}{2}\frac{\partial f_0(P)}{\partial P}\int_{u_{\rm dec}}^{u} ds e^{-i\hat{p}\cdot\hat{k}(s-u)}h'_k(s), \tag{B.16}$$

where we introduce the dimensionless variable $u = k\tau$.

Simultaneously, the stress-energy tensor can be expressed in terms of the distribution function $f(\mathbf{x},\mathbf{p},t)$:

$$T^{\nu}_{ij} = \frac{1}{\sqrt{-g}}\int\frac{d^3k}{k_0}k_i k_j f_{\mathbf{k}}(\mathbf{p},t), \tag{B.17}$$

Version of June 26, 2024 – Created June 27, 2024 - 16:33

where g represents the determinant of the metric tensor. The energy perturbation is then:

$$\delta T^{\nu}_{ij} = a^{-4} \int \frac{d^3k}{k_0} \left(\bar{k}_i \bar{k}_j \delta f + (\bar{k}_i \delta k_j + \bar{k}_j \delta k_i) f_0 \right). \tag{B.18}$$

Combining this equation with Eq.(B.16), and taking into account that the last two terms vanish in the first-order expansion, we arrive at:

$$\pi_{\lambda,\mathbf{k}} \epsilon^{\lambda}_{ij}(\mathbf{x}) = \frac{1}{2a^4} \int \frac{d^3p}{p^2} \frac{\partial f_0(P)}{\partial P} p_i p_j p_k p_l \int_{u_{\rm dec}}^{u} ds e^{-i\hat{p}\cdot\hat{k}(s-u)} h'_{\mathbf{k}}(s). \tag{B.19}$$

We also use the following formula:

$$\int d^3p\, p^{-2} p_i p_j p_k p_l e^{-i\hat{p}\cdot\hat{k}u} \epsilon^{\lambda}_{kl} = \frac{1}{4} \int d^3p\, p^{-4} (1 - 2\mu^2 + \mu^4) e^{-i\mu u} \epsilon^{\lambda}_{ij}, \tag{B.20}$$

where we applied the properties of tensor ϵ^{λ}_{kl} and introduced $\mu = \cos\theta = \hat{p}\cdot\hat{k}$. Finally, the anisotropic stress is given by:

$$\pi_{\mathbf{k}} = \frac{1}{4a^2} \int d^3p p (1 - 2\mu^2 + \mu^4) f_{\mathbf{k}}(\mathbf{p}, u). \tag{B.21}$$

By integrating in spherical coordinates by parts and using the identity:

$$\frac{1}{16} \int_{-1}^{1} d\mu (1 - 2\mu^2 + \mu^4) e^{-i\mu u} = \frac{j_2(u)}{u^2}, \tag{B.22}$$

we obtain the expression for the anisotropic part of the stress-energy tensor:

$$\pi_{\mathbf{k}} = -4\bar{\rho}_{\nu}(u) \int_{u_{\rm dec}}^{u} ds \frac{j_2(u-s)}{(u-s)^2} h'_{\mathbf{k}}(s), \tag{B.23}$$

where $\bar{\rho}_{\nu}(u) = a^{-4} \int d^3p p f_0(p)$.

Given the expression for the anisotropic part of the stress-energy tensor, we can derive the equation for tensor fluctuations:

$$h''_{ij} + 2\frac{a'(u)}{a} h'_{ij}(u) + h_{ij}(u) = -24 f_{\nu} \left(\frac{a'(u)}{a} \right)^2 \int_{u_{\rm dec}}^{u} \frac{j_2(u-s)}{(u-s)^2} h'_{ij}(s) ds, \tag{B.24}$$

where the neutrino fraction in the total energy density $f_{\nu}(u)$ is defined as:

$$f_{\nu}(u) = \frac{\bar{\rho}_{\nu}(u)}{\bar{\rho}(u)} = \frac{f_{\nu}(0)}{1 + a(u)/a_{\rm eq}}. \tag{B.25}$$

Version of June 26, 2024 – Created June 27, 2024 - 16:33

Its initial value is [28]:

$$f_\nu(0) = \frac{\Omega_\nu}{\Omega_\nu + \Omega_\gamma} = 0.40523. \tag{B.26}$$

Introducing the transfer function $\mathcal{T}(u)$ as

$$h_{ij}(u) = h_{ij}(0)\mathcal{T}(u), \tag{B.27}$$

we can write the equation for $\mathcal{T}(u)$:

$$\mathcal{T}''(u) + 2\frac{a'(u)}{a}\mathcal{T}'(u) + \mathcal{T}(u) = -24 f_\nu \left(\frac{a'(u)}{a}\right)^2 \int_{u_{\rm dec}}^{u} \frac{j_2(u-s)}{(u-s)^2}\mathcal{T}'(s)ds. \tag{B.28}$$

Before entering the horizon, perturbations do not evolve in time. Their amplitude is the same as it was at the end of inflation [16, 28]. These properties define the initial conditions for Eq.(B.28):

$$\mathcal{T}(0) = 1, \qquad \mathcal{T}'(0) = 0. \tag{B.29}$$

Version of June 26, 2024 – Created June 27, 2024 - 16:33

Appendix C

Transfer functions

This appendix provides solutions for the gravitational wave equation (2.14) in the absence of anisotropic stress. Perturbation amplitudes during different cosmological phases are [52]:

$$h_{\mathbf{k}}(\tau) = \begin{cases} \sqrt{\frac{16\pi G}{2k}}\frac{1}{a}\left(1-\frac{i}{k\tau}\right)e^{-ik\tau}\alpha(\mathbf{k}) & \text{de Sitter inflation,} \\ j_0(k\tau)h_{\text{prim}}(k) & \text{radiation domination,} \\ \frac{3j_1(k\tau)}{k\tau}h_{\text{prim}}(k) & \text{matter domination,} \end{cases} \tag{C.1}$$

where $\alpha(\mathbf{k})$ is a function normalized by $\langle\alpha(\mathbf{k})\alpha^*(\mathbf{k}')\rangle = \delta^3(\mathbf{k}-\mathbf{k}')$.

Amplitudes for modes outside the horizon $k\tau \ll 1$ are time-independent and their dimensionless power spectrum is:

$$\Delta^2_{GW}(k) \equiv 4k^3\frac{|h_{\text{prim}}(k)|^2}{2\pi^2} = \frac{64\pi G}{(2\pi)^2}H^2_{\text{inf}}\left(\frac{k\tau}{2\pi}\right)^2\left(1+\frac{1}{k^2\tau^2}\right) \approx \frac{2}{\pi^2}\left(\frac{H_{\text{inf}}}{M_{\text{Pl}}}\right)^2, \tag{C.2}$$

where we inserted the amplitude at the end of inflation $h_{\text{prim}}(k)$ from Eq.(C.1). This quantity depends on the inflation potential $V(\varphi)$ through Hubble parameter:

$$\Delta^2_{GW}(k) = \frac{2}{\pi^2}\left(\frac{H_{\text{inf}}}{M_{\text{Pl}}}\right)^2 = \frac{5V(\varphi)}{32\pi^2M^4_{Pl}}. \tag{C.3}$$

In the exponential inflation scenario, $\Delta^2_{GW}(k)$ is scale invariant.

The amplitude $h_{\lambda,\mathbf{k}}(\tau)$, within the formalism of transfer function, behaves as:

$$\mathcal{T}(k\tau) = \begin{cases} j_0(k\tau) & \tau < \tau_{\text{eq}}, k > k_{\text{eq}}, \\ \frac{\tau_{\text{eq}}}{\tau}\left[A(k)j_1(k\tau)+B(k)y_1(k\tau)\right] & \tau > \tau_{\text{eq}}, k > k_{\text{eq}}, \\ \frac{3j_1(k\tau)}{k\tau} & k < k_{\text{eq}}. \end{cases} \tag{C.4}$$

Version of June 26, 2024 – Created June 27, 2024 - 16:33

where $k_{\mathrm{eq}} = \tau_{\mathrm{eq}}^{-1}$ is the wavenumber corresponding to the moment of matter-radiation equality.

The derivatives of the transfer function $\mathcal{T}$ are:

$$\mathcal{T}'(k\tau) = \begin{cases} -kj_1(k\tau) & \tau < \tau_{\mathrm{eq}}, k > k_{\mathrm{eq}}, \\ -k\frac{\tau_{\mathrm{eq}}}{\tau}\left[A(k)j_2(k\tau) + B(k)y_2(k\tau)\right] & \tau > \tau_{\mathrm{eq}}, k > k_{\mathrm{eq}}, \\ -3\frac{j_2(k\tau)}{\tau} & k < k_{\mathrm{eq}}. \end{cases} \tag{C.5}$$

Matching the solutions at matter-radiation equality τ_{eq} provides coefficients $A(k)$ and $B(k)$:

$$A(k) = \frac{3}{2k\tau_{\mathrm{eq}}} - \frac{\cos 2k\tau_{\mathrm{eq}}}{2k\tau_{\mathrm{eq}}} + \frac{\sin 2k\tau_{\mathrm{eq}}}{(k\tau_{\mathrm{eq}})^2}, \tag{C.6}$$

$$B(k) = -1 + \frac{1}{(k\tau_{\mathrm{eq}})^2} - \frac{\cos 2k\tau_{\mathrm{eq}}}{(k\tau_{\mathrm{eq}})^2} - \frac{\sin 2k\tau_{\mathrm{eq}}}{2k\tau_{\mathrm{eq}}}. \tag{C.7}$$

Version of June 26, 2024 – Created June 27, 2024 - 16:33

Appendix D

Relative spectral density

In this appendix, we derive the energy density of gravitational waves, following Misner, Thorne, and Wheeler [53].

We start by expanding the Ricci curvature tensor $R_{\mu\nu}$ in perturbations h:

$$R_{\mu\nu} = \bar{R}_{\mu\nu} + R^{(1)}_{\mu\nu} + R^{(2)}_{\mu\nu} + O(h^3). \tag{D.1}$$

n vacuum, with no sources of perturbations, $R_{\mu\nu} = 0$. Due to the nonlinearity of Einstein's equations, the linear term disappears:

$$R^{(1)\text{linear}}_{\mu\nu} = 0. \tag{D.2}$$

This is the same as Eq. (2.14).

The remaining terms can be divided into high-frequency (large-scale) and long-frequency (small-scale) modes. For the former, gravitational waves are the source of curvature:

$$\bar{R}_{\mu\nu} + \langle R^{(2)}_{\mu\nu} \rangle = 0. \tag{D.3}$$

The small-scale part fluctuates due to propagation through matter:

$$R^{(1)\text{nonlinear}}_{\mu\nu} + R^{(2)}_{\mu\nu} - \langle R^{(2)}_{\mu\nu} \rangle = 0. \tag{D.4}$$

Einstein equations,

$$G_{\mu\nu} = R_{\mu\nu} - \frac{1}{2} R g_{\mu\nu} = 8\pi G T^{(\text{GW})}_{\mu\nu}, \tag{D.5}$$

result into:

$$T^{(\text{GW})}_{\mu\nu} \equiv -\frac{1}{8\pi G} \left(\langle R^{(2)}_{\mu\nu} \rangle - \frac{1}{2} g_{\mu\nu} \langle R^{(2)} \rangle \right). \tag{D.6}$$

The Ricci tensor in the linearized theory is [17]:

$$R^{(2)}_{\mu\nu} = \frac{1}{2}\bar{g}^{\rho\sigma}\bar{g}^{\alpha\beta}\Big[\frac{1}{2}h_{\rho\alpha|\mu}h_{\sigma\beta|\nu} + h_{\nu\alpha|\rho}(h_{\mu\beta|\sigma} - h_{\mu\sigma|\beta}) + \\ + h_{\rho\alpha}(h_{\sigma\beta|\nu\mu} + h_{\mu\nu|\beta\sigma} - h_{\mu\sigma|\beta\nu} - h_{\nu\sigma|\beta\mu}) + \\ + \left(\frac{1}{2}h_{\rho\sigma|\alpha} - h_{\alpha\sigma|\rho}\right)(h_{\mu\beta|\nu} + h_{\nu\beta|\mu} - h_{\mu\nu|\beta})\Big], \tag{D.7}$$

where $|$ denotes the covariant derivative with respect to the unperturbed metric.

Averaging over several wavelengths and using integration by parts, while accounting for the equation of motion $\Box h_{\mu\nu} = 0$, Lorentz gauge $\partial_\mu h^{\mu\nu} = 0$, and tracelessness $h = 0$, we obtain:

$$\langle R^{(2)}_{\mu\nu}\rangle = -\frac{1}{4}\langle h_{\alpha\beta|\mu}h^{\alpha\beta}_{\ \ |\nu}\rangle. \tag{D.8}$$

Then stress-energy tensor for gravitational waves is:

$$T^{(\mathrm{GW})}_{\mu\nu} = \frac{1}{32\pi G}\langle h_{\alpha\beta|\mu}h^{\alpha\beta}_{\ \ |\nu}\rangle = \frac{1}{32\pi G}\langle h_{\alpha\beta,\mu}h^{\alpha\beta}_{\ \ ,\nu}\rangle + O(h^3). \tag{D.9}$$

The energy density of gravitational waves in the TT gauge is:

$$\rho_{GW}(\tau) \equiv T^{(\mathrm{GW})}_{00} = \frac{1}{32\pi G a^2(\tau)}\langle h'_{ij}h'^{ij}\rangle. \tag{D.10}$$

The independent modes of gravitational waves, which are conventionally denoted $+$ and $\times$, moving in z direction, are:

$$h_{ij} = \begin{pmatrix} h_+ & h_\times & 0 \\ h_\times & -h_+ & 0 \\ 0 & 0 & 0 \end{pmatrix}. \tag{D.11}$$

As a result,

$$\rho_{GW}(\tau) = \frac{1}{16\pi G a^2}\langle h'^2_+ + h'^2_\times\rangle = \frac{1}{16\pi G a^2}\int\frac{d^3k}{(2\pi)^3}\int\frac{d^3k'}{(2\pi)^3}\langle(h'_{+,\mathbf{k}}h'_{+,\mathbf{k}'} + \\ + h'_{\times,\mathbf{k}}h'_{\times,\mathbf{k}'})e^{i(k+k')\cdot x}\rangle, \tag{D.12}$$

where we used Fourier transform $h^*_{\lambda,\mathbf{k}} = h_{\lambda,-\mathbf{k}}$.

Version of June 26, 2024 – Created June 27, 2024 - 16:33

Averaging over a range of wavelengths is equivalent to ensemble averaging:

$$\langle h'_{\lambda,\mathbf{k}} h'_{\lambda',\mathbf{k}'} \rangle = (2\pi)^3 \delta_{\lambda,\lambda'} \delta^{(3)}(\mathbf{k}+\mathbf{k}') |h'_{\lambda,\mathbf{k}}|^2, \tag{D.13}$$

we get:

$$\rho_{GW}(\tau) = \frac{1}{16\pi G a^2} \int \frac{d^3k}{(2\pi)^3} \left[|h'_{+,\mathbf{k}}(\tau)|^2 + |h'_{\times,\mathbf{k}}(\tau)|^2 \right]. \tag{D.14}$$

For unpolarized primordial spectra $|h_{\times,\mathbf{k}}|^2 = |h_{+,\mathbf{k}}|^2$, we obtain:

$$\rho_{GW}(\tau) = \frac{1}{32\pi G a^2} \int d\ln k \Delta^2_{h,\mathrm{prim}} \left[T'(k\tau) \right]^2, \tag{D.15}$$

where we applied definitions of transfer function $T(k\tau)$ and primordial spectra $\Delta^2_{GW,\mathrm{prim}}$:

$$\Delta^2_{GW,\mathrm{prim}} \equiv 4 \frac{k^3}{2\pi^2} |h_{\mathrm{prim}}(k)|^2 = \frac{16}{\pi} \left(\frac{H_{\mathrm{inf}}}{m_{\mathrm{Pl}}} \right)^2. \tag{D.16}$$

For superhorizon modes ($|k\tau| \ll 1$), the amplitude is $|h_{\mathrm{prim}}(k)|^2$ as it was during inflation. For subhorizon modes ($|k\tau| \gg 1$), the evolution of the power spectra $[T'(k\tau)]^2$ is defined by $[T'(k\tau)]^2$. This factor behaves as $\tau^{-2} \propto a^{-2}$ at the radiation era and $\propto \tau^{-4} \propto a^{-2}$ during the matter era. Hence, $\rho_{GW} \propto a^{-4}$, indicating that gravitational waves are radiation (gravitons are massless particles).

The relative spectral density is:

$$\Omega_{GW}(\tau, k) \equiv \frac{\tilde{\rho}_{GW}(\tau, k)}{\rho_{\mathrm{cr}}(\tau)}, \tag{D.17}$$

where $\tilde{\rho}_{GW}(\tau, k)$ is the energy density per logarithmic scale:

$$\tilde{\rho}_{GW}(\tau, k) \equiv \frac{d\rho_{GW}(\tau)}{d\ln k}. \tag{D.18}$$

Here, $\rho_{\mathrm{cr}}(\tau)$ denotes the critical density of the Universe.

Combining this definition with Eq. (D.15), we get:

$$\Omega_{GW}(\tau, k) = \frac{\Delta^2_{GW,\mathrm{prim}}}{32\pi G a^2 \rho_{\mathrm{cr}}(\tau)} \left[T'(\tau, k) \right]^2. \tag{D.19}$$

Or,

$$\Omega_{GW}(\tau, k) = \frac{\Delta^2_{GW,\mathrm{prim}}}{12 H^2(\tau) a^2} \left[T'(\tau, k) \right]^2, \tag{D.20}$$

where we used $H^2 = \frac{8\pi G \rho_{\mathrm{cr}}}{3}$.

Version of June 26, 2024 – Created June 27, 2024 - 16:33

Appendix E

Temperature evolution

In this appendix we derive the Eq.(5.25), beginning with the energy conservation:

$$T d(\rho_R a^3) = -p_R d(a^3) + \Gamma_\varphi \rho_\varphi a^3 dt. \tag{E.1}$$

By applying the definition of entropy (3.3), this equation is transformed to:

$$\frac{1}{a^3}\frac{d(s_R a^3)}{dt} = \frac{\Gamma_\varphi \rho_\varphi}{T}. \tag{E.2}$$

$$3H(a)s_R + \frac{ds_R}{dt} = \frac{\Gamma_\varphi \rho_\varphi}{T}. \tag{E.3}$$

Using the temperature dependency of entropy (3.1), the derivative becomes:

$$\frac{ds_R}{dt} = \frac{2\pi^2}{45}\left(\frac{dg_{\star,s}}{dT}T^3 + 3g_{\star,s}T^2\right)\frac{dT}{dt}. \tag{E.4}$$

Substituting this into Eq.(E.2), we get:

$$3H(a)s_R + \frac{2\pi^2}{45}\left(\frac{dg_{\star,s}}{dT}T^3 + 3g_{\star,s}T^2\right)\frac{dT}{dt} = \frac{\Gamma_\varphi \rho_\varphi}{T}. \tag{E.5}$$

Eliminating the time t from the equation results in

$$3H(a)s_R + \frac{2\pi^2}{45}H(a)a\left(\frac{dg_{\star,s}}{dT}T^3 + 3g_{\star,s}T^2\right)\frac{dT}{da} = \frac{\Gamma_\varphi \rho_\varphi}{T}. \tag{E.6}$$

This leads to the final equation for temperature evolution:

$$\frac{dT}{da} = \left[1 + \frac{T}{3g_{\star,s}}\frac{dg_{\star,s}}{dT}\right]^{-1}\left[-\frac{T}{a} + \frac{\Gamma_\varphi \rho_\varphi}{3H(a)s_R(T)a}\right]. \tag{E.7}$$

Version of June 26, 2024 – Created June 27, 2024 - 16:33

Bibliography

[1] Richard H. Cyburt, Brian D. Fields, Keith A. Olive, and Tsung-Han Yeh. Big Bang Nucleosynthesis: 2015. *Rev. Mod. Phys.*, 88:015004, 2016.

[2] R. L. Workman et al. Review of Particle Physics. *PTEP*, 2022:083C01, 2022.

[3] N. Aghanim et al. Planck 2018 results. VI. Cosmological parameters. *Astron. Astrophys.*, 641:A6, 2020. [Erratum: Astron.Astrophys. 652, C4 (2021)].

[4] Alexei A. Starobinsky. Dynamics of Phase Transition in the New Inflationary Universe Scenario and Generation of Perturbations. *Phys. Lett. B*, 117:175–178, 1982.

[5] Andrei D. Linde. A New Inflationary Universe Scenario: A Possible Solution of the Horizon, Flatness, Homogeneity, Isotropy and Primordial Monopole Problems. *Phys. Lett. B*, 108:389–393, 1982.

[6] Alan H. Guth. The Inflationary Universe: A Possible Solution to the Horizon and Flatness Problems. *Phys. Rev. D*, 23:347–356, 1981.

[7] Andrei D. Linde. Scalar Field Fluctuations in Expanding Universe and the New Inflationary Universe Scenario. *Phys. Lett. B*, 116:335–339, 1982.

[8] Alan H. Guth and S. Y. Pi. Fluctuations in the New Inflationary Universe. *Phys. Rev. Lett.*, 49:1110–1113, 1982.

[9] James M. Bardeen, Paul J. Steinhardt, and Michael S. Turner. Spontaneous Creation of Almost Scale - Free Density Perturbations in an Inflationary Universe. *Phys. Rev. D*, 28:679, 1983.

[10] Y. Akrami et al. Planck 2018 results. X. Constraints on inflation. *Astron. Astrophys.*, 641:A10, 2020.

[11] Varun Sahni. The Energy Density of Relic Gravity Waves From Inflation. *Phys. Rev. D*, 42:453–463, 1990.

[12] L. P. Grishchuk and Yu. V. Sidorov. Squeezed quantum states of relic gravitons and primordial density fluctuations. *Phys. Rev. D*, 42:3413–3421, 1990.

[13] Bruce Allen. The Stochastic Gravity Wave Background in Inflationary Universe Models. *Phys. Rev. D*, 37:2078, 1988.

[14] Dominik J. Schwarz. Evolution of gravitational waves through cosmological transitions. *Mod. Phys. Lett. A*, 13:2771–2778, 1998.

[15] Naoki Seto and Jun'Ichi Yokoyama. Probing the equation of state of the early universe with a space laser interferometer. *J. Phys. Soc. Jap.*, 72:3082–3086, 2003.

[16] Steven Weinberg. Damping of tensor modes in cosmology. *Phys. Rev. D*, 69:023503, 2004.

[17] Michele Maggiore. *Gravitational waves: Volume 1: Theory and experiments*. OUP Oxford, 2007.

[18] Marc Kamionkowski, Arthur Kosowsky, and Albert Stebbins. Statistics of cosmic microwave background polarization. *Phys. Rev. D*, 55:7368–7388, 1997.

[19] Shun Saito, Kiyotomo Ichiki, and Atsushi Taruya. Probing polarization states of primordial gravitational waves with CMB anisotropies. *JCAP*, 09:002, 2007.

[20] B. P. Abbott et al. Observation of Gravitational Waves from a Binary Black Hole Merger. *Phys. Rev. Lett.*, 116(6):061102, 2016.

[21] B. P. Abbott et al. Gravitational Waves and Gamma-rays from a Binary Neutron Star Merger: GW170817 and GRB 170817A. *Astrophys. J. Lett.*, 848(2):L13, 2017.

[22] S. Kawamura et al. The Japanese space gravitational wave antenna DECIGO. *Class. Quant. Grav.*, 23:S125–S132, 2006.

[23] Curt Cutler and Daniel E. Holz. Ultra-high precision cosmology from gravitational waves. *Phys. Rev. D*, 80:104009, 2009.

[24] Pau Amaro-Seoane et al. Laser Interferometer Space Antenna. 2 2017.

[25] Tristan L. Smith, Marc Kamionkowski, and Asantha Cooray. Direct detection of the inflationary gravitational wave background. *Phys. Rev. D*, 73:023504, 2006.

[26] Kai Schmitz. New Sensitivity Curves for Gravitational-Wave Signals from Cosmological Phase Transitions. *JHEP*, 01:097, 2021.

[27] M. C. Guzzetti, N. Bartolo, M. Liguori, and S. Matarrese. Gravitational waves from inflation. *Riv. Nuovo Cim.*, 39(9):399–495, 2016.

[28] Yuki Watanabe and Eiichiro Komatsu. Improved calculation of the primordial gravitational wave spectrum in the standard model. *Physical Review D*, 73(12):123515, 2006.

[29] Dmitry S Gorbunov and Valery A Rubakov. *Introduction to the theory of the early universe: Cosmological perturbations and inflationary theory*. World Scientific, 2011.

[30] Lars Husdal. On Effective Degrees of Freedom in the Early Universe. *Galaxies*, 4(4):78, 2016.

[31] Gianpiero Mangano, Gennaro Miele, S Pastor, and M Peloso. A precision calculation of the effective number of cosmological neutrinos. *Physics Letters B*, 534(1-4):8–16, 2002.

[32] Mark Hindmarsh and Owe Philipsen. Dark matter of weakly interacting massive particles and the qcd equation of state. *Physical Review D*, 71(8):087302, 2005.

[33] James E. Lidsey, Andrew R. Liddle, Edward W. Kolb, Edmund J. Copeland, Tiago Barreiro, and Mark Abney. Reconstructing the inflation potential : An overview. *Rev. Mod. Phys.*, 69:373–410, 1997.

[34] Marc Kamionkowski, Arthur Kosowsky, and Michael S. Turner. Gravitational radiation from first order phase transitions. *Phys. Rev. D*, 49:2837–2851, 1994.

[35] Nicolás Bernal and Fazlollah Hajkarim. Primordial Gravitational Waves in Nonstandard Cosmologies. *Phys. Rev. D*, 100(6):063502, 2019.

[36] Rouzbeh Allahverdi et al. The First Three Seconds: a Review of Possible Expansion Histories of the Early Universe. 6 2020.

[37] Sachiko Kuroyanagi, Takeshi Chiba, and Tomo Takahashi. Probing the Universe through the Stochastic Gravitational Wave Background. *JCAP*, 11:038, 2018.

[38] Andrei D. Linde. *Particle physics and inflationary cosmology*, volume 5. 1990.

[39] David H. Lyth and Antonio Riotto. Particle physics models of inflation and the cosmological density perturbation. *Phys. Rept.*, 314:1–146, 1999.

[40] Lev Kofman, Andrei D. Linde, and Alexei A. Starobinsky. Towards the theory of reheating after inflation. *Phys. Rev. D*, 56:3258–3295, 1997.

[41] Daniel Grin, Tristan L. Smith, and Marc Kamionkowski. Axion constraints in non-standard thermal histories. *Phys. Rev. D*, 77:085020, 2008.

[42] M. Kawasaki, Kazunori Kohri, and Naoshi Sugiyama. MeV scale reheating temperature and thermalization of neutrino background. *Phys. Rev. D*, 62:023506, 2000.

[43] Steen Hannestad. What is the lowest possible reheating temperature? *Phys. Rev. D*, 70:043506, 2004.

[44] Francesco De Bernardis, Luca Pagano, and Alessandro Melchiorri. New constraints on the reheating temperature of the universe after WMAP-5. *Astropart. Phys.*, 30:192–195, 2008.

[45] P. F. de Salas, M. Lattanzi, G. Mangano, G. Miele, S. Pastor, and O. Pisanti. Bounds on very low reheating scenarios after Planck. *Phys. Rev. D*, 92(12):123534, 2015.

[46] Thomas Kite, Jens Chluba, Andrea Ravenni, and Subodh P. Patil. Clarifying transfer function approximations for the large-scale gravitational wave background in ΛCDM. *Mon. Not. Roy. Astron. Soc.*, 509(1):1366–1376, 2021.

[47] Ken'ichi Saikawa and Satoshi Shirai. Primordial gravitational waves, precisely: The role of thermodynamics in the Standard Model. *JCAP*, 05:035, 2018.

[48] Takehiko Asaka and Mikhail Shaposhnikov. The νMSM, dark matter and baryon asymmetry of the universe. *Phys. Lett. B*, 620:17–26, 2005.

[49] Takehiko Asaka, Steve Blanchet, and Mikhail Shaposhnikov. The nuMSM, dark matter and neutrino masses. *Phys. Lett. B*, 631:151–156, 2005.

[50] Kyrylo Bondarenko, Alexey Boyarsky, Dmitry Gorbunov, and Oleg Ruchayskiy. Phenomenology of GeV-scale Heavy Neutral Leptons. *JHEP*, 11:032, 2018.

[51] Ernest Ma. Pathways to naturally small neutrino masses. *Phys. Rev. Lett.*, 81:1171–1174, 1998.

[52] N. D. Birrell and P. C. W. Davies. *Quantum Fields in Curved Space*. Cambridge Monographs on Mathematical Physics. Cambridge Univ. Press, Cambridge, UK, 2 1984.

[53] Charles W. Misner, K. S. Thorne, and J. A. Wheeler. *Gravitation*. W. H. Freeman, San Francisco, 1973.